GEOLOGICA CARPATHICA, JUNE 2018, 69, 3, 237–253 doi: 10.1515/geoca-2018-0014

The Oligocene Reifnitz tonalite (Austria) and its host rocks: implications for Cretaceous and Oligocene–Neogene tectonics of the south-eastern Eastern Alps

FRANZ NEUBAUER[1,✉], BIANCA HEBERER[1], ISTVÁN DUNKL[2], XIAOMING LIU[3], MANFRED BERNROIDER[1] and YUNPENG DONG[3]

[1]Department of Geography and Geology, University of Salzburg, Hellbrunner Str. 34, A-5020 Salzburg, Austria; ✉Franz.Neubauer@sbg.ac.at
[2]Sedimentology and Environmental Geology, Geoscience Centre, University of Göttingen, Goldschmidtstrasse 3, D-37077 Göttingen, Germany
[3]State Key Laboratory of Continental Dynamics, Department of Geology, Northwest University, Xi'an 710069, China

(Manuscript received August 5, 2017; accepted in revised form May 11, 2018)

Abstract: In the south-eastern Eastern Alps, the Reifnitz tonalite intruded into the Austroalpine metamorphic basement of the Wörthersee half-window exposed north of the Sarmatian–Pliocene flexural Klagenfurt basin. The Reifnitz tonalite is dated for the first time, and yields a laser ICP-MS U–Pb zircon age of 30.72±0.30 Ma. The (U–Th–Sm)/He apatite age of the tonalite is 27.6±1.8 Ma implying rapid Late Oligocene cooling of the tonalite to ca. 60 °C. The Reifnitz tonalite intruded into a retrogressed amphibolite-grade metamorphic basement with a metamorphic overprint of Cretaceous age ($^{40}Ar/^{39}Ar$ white mica plateau age of 90.7±1.6 Ma). This fact indicates that pervasive Alpine metamorphism of Cretaceous age extends southwards almost up to the Periadriatic fault. Based on the exhumation and erosion history of the Reifnitz tonalite and the hosting Wörthersee half window formed by the Wörthersee anticline, the age of gentle folding of Austroalpine units in the south-eastern part of the Eastern Alps is likely of Oligocene age. North of the Wörthersee antiform, Upper Cretaceous–Eocene, Oligocene and Miocene sedimentary rocks of the Krappfeld basin are preserved in a gentle synform, suggesting that the top of the Krappfeld basin has always been near the Earth's surface since the Late Cretaceous. The new data imply, therefore, that the Reifnitz tonalite is part of a post-30 Ma antiform, which was likely exhumed, uplifted and eroded in two steps. In the first step, which is dated to ca. 31–27 Ma, rapid cooling to ca. 60 °C and exhumation occurred in an E–W trending antiform, which formed as a result of a regional N–S compression. In the second step of the Sarmatian–Pliocene age a final exhumation occurred in the peripheral bulge in response to the lithospheric flexure in front of the overriding North Karawanken thrust sheet. The Klagenfurt basin developed as a flexural basin at the northern front of the North Karawanken, which represent a transpressive thrust sheet of a positive flower structure related to the final activity along the Periadriatic fault. In the Eastern Alps, on a large scale, the distribution of Periadriatic plutons and volcanics seems to monitor a northward or eastward shift of magmatic activity, with the main phase of intrusions ca. 30 Ma at the fault itself.

Keywords: Periadriatic magmatism, peripheral bulge, exhumation, cooling history, shortening.

Introduction

Intrusion of plutons during the late-stage orogenic processes is of high importance for several reasons. Such plutons often provide evidence of plate tectonic processes such as subduction, break-off or delamination of the subducted oceanic slab (e.g., von Blanckenburg & Davies 1995; von Blanckenburg et al. 1998; Seghedi & Downes 2012) or simply decompressional melting of the exhuming, previously subducted crust (Brown 2013). Plutons are often aligned along crustal-scale faults like the Periadriatic fault (Schmid et al. 1987, 1989; Rosenberg 2004; Handy et al. 2015; Cao & Neubauer 2016 and references therein). This may lead to rheological decoupling of different portions of the orogenic crust, influencing therefore, the large-scale structure of mountain belts (Fig. 1). Finally, deciphering exhumation paths of such plutons may add to the reconstruction of vertical motion of the intruded crust along these major fault zones (e.g., Rosenberg 2004 and references therein; Cao & Neubauer 2016).

Here, we report new data (U–Pb zircon age, microprobe data of garnet) from the hitherto undated Reifnitz tonalite from the south-eastern part of the Eastern Alps. This tonalite was not considered in recent geodynamic models as its age and significance were unknown (e.g., Rosenberg 2004). The U–Pb zircon and (U–Th)/He ages in combination with the first $^{40}Ar/^{39}Ar$ white mica age from the host rock and available regional geological data from adjacent sedimentary basins allow us to propose a major event of gentle N–S shortening by folding and associated erosion for this sector of the Eastern Alps, which was not known before. We also discuss the large-scale distribution of Oligocene to Miocene Periadriatic plutons, which clearly shows a northward or eastward shift of magmatic activity, and discuss the potential significance.

Geological setting

In the Eastern Alps, the European plate constitutes the lower plate subducted principally beneath the overriding north-directed Austroalpine nappe complex and other elements of the Alpine orogenic wedge (Fig. 1) during Late Cretaceous to Oligocene times. The Austroalpine nappe complex is a detached part of the Adriatic microplate and is exposed north of the Periadriatic fault. The Southern Alps and Dinarides have a Paleogene to recent southward and south-westward vergency towards Adria, which is commonly explained as back-thrusting to the principally S-directed subduction polarity of the European plate (e.g., TRANSALP Working Group 2002 and a contrary view in Lippitsch et al. 2003). The pattern is superposed by Oligocene–Miocene eastward extrusion of the ALCAPA (Alpine–Carpathian–Pannonian) block north of the Periadriatic fault (Kázmér & Kovács 1985; Ratschbacher et al. 1989, 1991), which is associated with Periadriatic plutons (Rosenberg 2004 and references therein). On a large scale, the Periadriatic plutons are aligned along the Periadriatic fault (Fig. 1) and allowed shear concentration by rheological weakening of the crust.

The south-eastern Austroalpine nappe complex north of the Periadriatic fault (Fig. 2) is composed mostly of partly retrogressed and potentially polymetamorphic micaschists of the metamorphosed Middle Austroalpine basement ("Altkristallin" in the older terminology) covered by the Stangalm Permo–Mesozoic cover unit (von Gosen 1989). This unit is overridden by the Gurktal nappe complex, which contains two major subunits with Ordovician to Lower Carboniferous successions, the lower Murau nappe with mainly phyllites and the upper Stolzalpe nappe with mainly slate and mafic volcanics and subordinate thin limestones and dolomites. This unit is covered by unmetamorphic to very low-grade Permian to Triassic successions, such as the Eberstein Permo–Triassic (Fig. 2) (Appold & Pesch 1984). The boundary between the Middle Austroalpine unit and the Gurktal nappe complex is a top-WNW ductile thrust fault overprinted by a Late Cretaceous top-ESE ductile normal fault causing retrogression of micaschists along the ductile normal fault (e.g., Ratschbacher et al. 1989; Koroknai et al. 1999). Normal faulting was associated with the formation of the Santonian to Eocene Krappfeld Gosau basin (Koroknai et al. 1999; Willingshofer et al. 1999).

The overall structure of the southernmost sectors of Austroalpine units is less clear, particularly along the south-eastern portion within the study area south of Lake Wörthersee (Figs. 2, 3), which has been described as the Klagenfurt (or

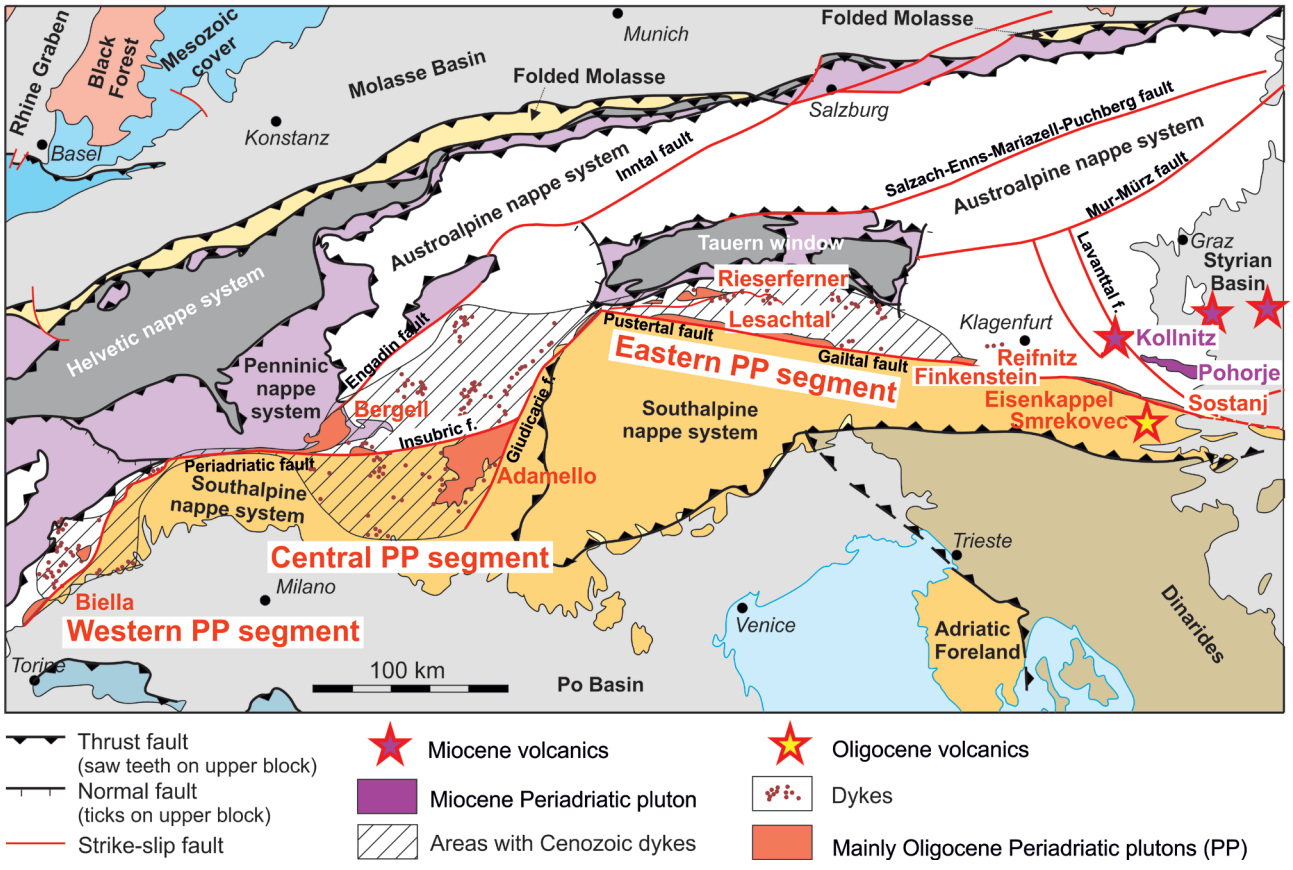

Fig. 1. Simplified geology of the Alps (after Pfiffner 2014 and Neubauer 2014) showing the distribution of Eocene to Miocene Periadriatic plutons, dykes and volcanics (modified after Rosenberg 2004).

Wörthersee) half-window (e.g., Claasen et al. 1987; von Gosen 1989). There, amphibolite-grade, in part retrogressed mica-schists are exposed (Schwaighofer 1965; von Gosen 1989). These units also extend north of Lake Wörthersee (Homann 1962) in ca. E–W striking tectonic windows underneath the Gurktal nappe complex (Kleinschmidt et al. 2008).

It has been known for a long time, that small scattered bodies of tonalite are exposed within the "Altkristallin" basement north of the not well studied E–W trending Keutschach fault over a length of about eight kilometres (e.g., Kahler 1931, 1953, 1962; Meixner 1949; Heritsch 1964, 1971; Schwaighofer 1965). Along the Keutschach fault, low-grade Permo–Mesozoic units are exposed including the Viktring Permo–Mesozoic (Schünemann et al. 1982) and the Rossegg Permo–Mesozoic units (Claasen et al. 1987) (Figs. 2, 3), which correlate either with the Stangalm Permo–Mesozoic underneath the Gurktal nappe system or with the Eberstein Permo–Mesozoic above it. Further to the east, small remnants of Permo–Mesozoic formations are exposed between Klagenfurt and Völkermarkt (Fig. 2). The Viktring and Rossegg Permo–Mesozoic units have mostly undergone Cretaceous low-grade metamorphism (von Gosen et al. 1987). In spite of their metamorphic overprint, Claasen et al. (1987) suggested that these units belong to the cover of the Gurktal nappe complex rather than being a correlative unit of the Stangalm Permo–Mesozoic unit.

All these units are overlain (Fig. 3) by the uppermost Middle Miocene to Pliocene Sattnitz Conglomerate, which is overlying, at Penken, the potentially Middle Miocene "Ground Seam" Formation ("Grundflöz" strata composed of terrestrial mudstone and coals (Kahler 1929; Griem et al. 1991). Kahler (1929, 1931) found Middle Miocene agglutinated foraminifera within basal mudstones implying a short marine ingression. However, this observation was not confirmed later because of the lack of exposures since cessation of coal mining.

Eocene to Miocene (42–14 Ma) plutons, dykes and volcanics of mainly intermediate and rare mafic composition are widespread along the Periadriatic fault (Fig. 1; Deutsch 1984; Dal Piaz et al. 1988; von Blanckenburg et al. 1998; Rosenberg 2004; D´Adda et al. 2011; Bergomi et al. 2015). It was proposed that they comprise two age groups: ca. 42–30 Ma old plutons and dykes in the west, and ca. 30–14 Ma old volcanics

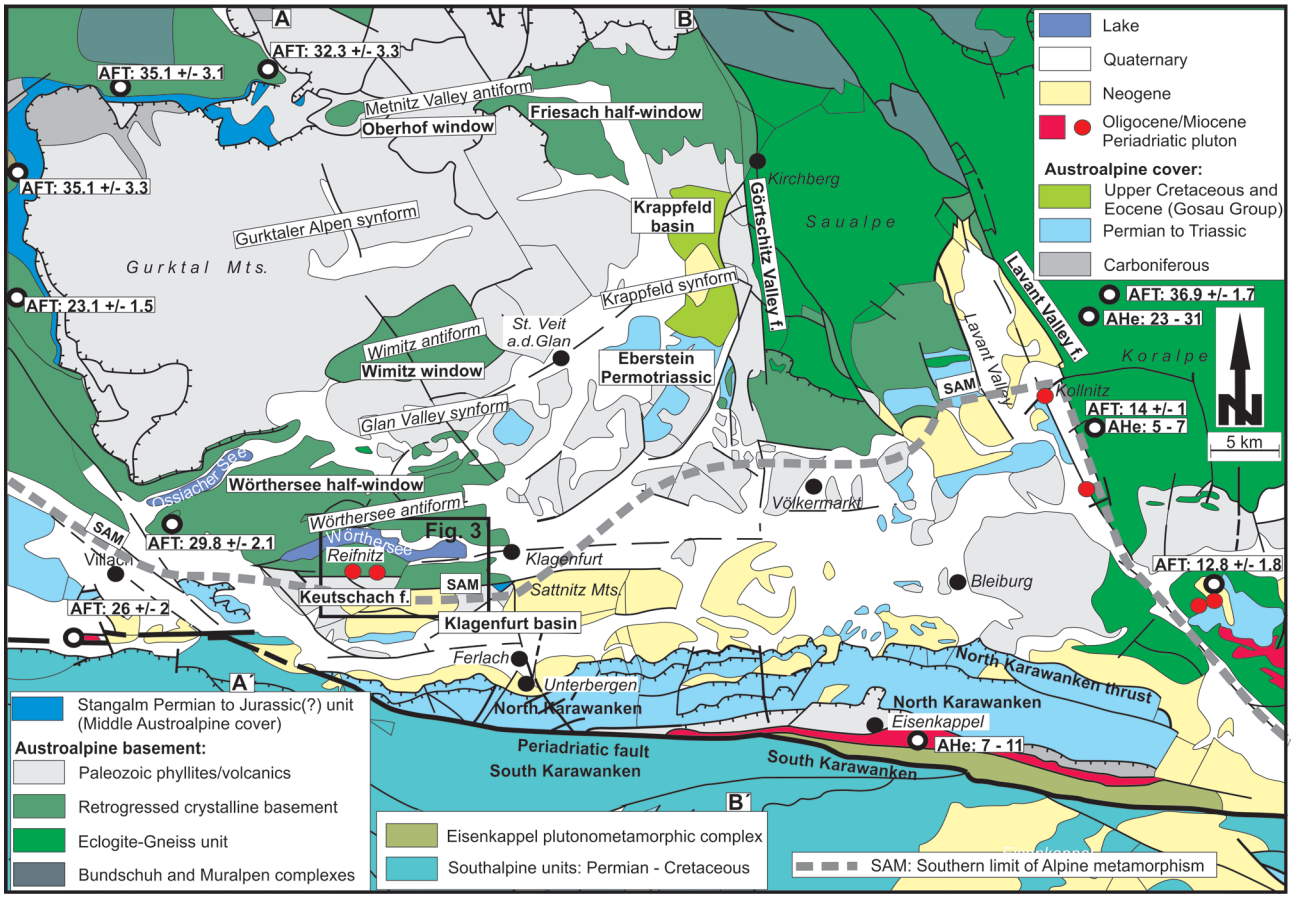

Fig. 2. Geological map of the south-eastern Alps (modified after Bigi et al. 1990) and apatite fission track and (U–Th)/He ages. A–A´and B–B´are locations of N–S sections shown in Figure 11. Sources for apatite fission track ages (AFT) and (U–Th)/He (AHe) ages: Hejl (1997), Sachsenhofer et al. (1998), Wölfler et al. (2010), Kurz et al. (2011), Legrain et al. (2014) and Heberer et al. (2017). The orientation of lettering of various synforms and antiforms gives fold orientation.

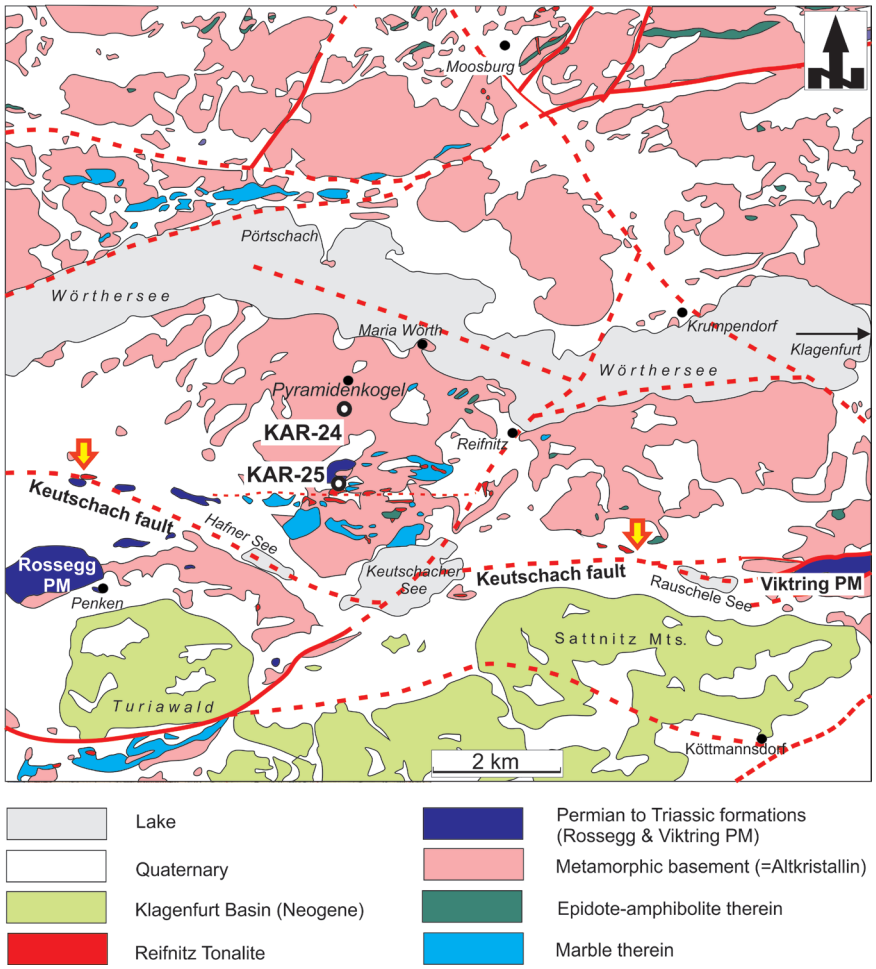

Fig. 3. Simplified geological map of the Wörthersee region with location of the study area (modified after Kahler 1962). Red-yellow arrows indicate westernmost and easternmost exposures of the Reifnitz tonalite.

and subordinate plutons in the east (Fodor et al. 1998, 2008; Hanfland et al 2004; Kralj 2012, 2013). Based on the widespread occurrence of these plutons, Late Eocene to Oligocene slab break-off of the subducted oceanic lithosphere from the subducted European continental plate during plate collision and uprise of hot asthenosphere through the slab window of the broken subducted plate has been postulated (von Blanckenburg & Davies 1995; von Blanckenburg et al. 1998). The main period of magmatism occurred at ca. 34–30 Ma. In the Eastern Alps, however, much younger periods of magmatism (18–14 Ma, ca. 11–1.6 Ma) are well known north of the Periadriatic fault implying younger magma-producing mantle processes (e.g., Lippolt et al. 1975; Deutsch 1980, 1984; Handler et al. 2006; Fodor et al. 2008; Trajanova et al. 2008 and references therein) independent from the classical 34–30 Ma slab-break off event sensu von Blanckenburg et al. (1995) and Davies & von Blanckenburg (1995). The second magmatic phase ranging from ca. 18–14 Ma (e.g., Ebner & Sachsenhofer 1995; Fodor et al. 2008; Trajanova et al. 2008) is not well explained in the slab break-off model (von Blanckenburg et al. 1998). Fodor et al. (2008) interpreted the Pohorje pluton as intruded in an E–W extensional setting related to strike-slip deformation along the Periadriatic fault.

Thermochronology can constrain the post-magmatic cooling of intrusions and post-metamorphic cooling of crust in mountain belts. Sparse apatite fission track (AFT) and few (U–Th–Sm)/He (AHe) ages are available from the Austroalpine nappe complex north of the Periadriatic fault (Hejl 1997, 1999; Heberer et al. 2017; Fig. 2), and only a few AFT and AHe ages are available from the eastern Periadriatic fault (Nemes 1997; Heberer et al. 2017; Fig. 2). An AFT age of the Villach granite gneiss is 29.8±2.1 Ma (Hejl 1997). AFT ages adjacent to the eastern Periadriatic fault mainly range from 15 to 25 Ma with an age of 23.1±1.5 Ma for the Finkenstein tonalite (Hejl 1997; Nemes 1997; Fodor et al. 2008) and (U–Th–Sm)/He ages from 6.3±1.0 to 11.4±1.1 Ma (Heberer et al. 2017). Dunkl et al. (2005) reported several populations of apatite fission track ages (36±14 Ma, 30±1 Ma, and 20±4 Ma) from two Miocene sandstones of the Klagenfurt basin interpreted as reflecting the denudation history of the source regions.

Analytical methods

Electron microprobe analytical technique

Well preserved garnet grains were analysed in polished thin sections by using a fully automated JEOL 8600 electron microprobe at the Dept. of Geography and Geology, University of Salzburg, Austria. Point analyses were obtained using a 15 kV accelerating voltage and 40 nA beam current. The beam size was set to 5 µm. Natural and synthetic oxides and silicates were used as standards for major elements. We used the Mathematica package based software (PET) (Dachs 2004) for mineral formula calculation.

U–Pb dating

The U–Pb analytical techniques largely follow those described in Liu et al. (2008). The zircon concentrate was prepared at the University of Salzburg. Zircons were dated *in-situ* on an excimer (193 nm wave length) laser ablation inductively coupled plasma mass spectrometer (LA-ICP-MS) at the State Key Laboratory of Continental Dynamics,

Northwest University, Xi´an, China. The ICP-MS used is an Agilent 7500a (with shield torch). The unique shield torch increases analytical sensitivity by a factor of >10, (for example, 4500 cps/ppm for ^{238}U at a spot size of 40 µm and laser frequency of 10 Hz), which is important for LA-ICP-MS. The GeoLas 200M laser ablation system (MicroLas, Göttingen, Germany) was used for the laser ablation experiments. Helium was used as carrier gas. The used spot size and laser frequency were 40 µm and 10 Hz, respectively. The data acquisition mode was peak jumping (20 ms per isotope each cycle). Raw count rates were measured for ^{29}Si, ^{204}Pb, ^{206}Pb, ^{207}Pb, ^{208}Pb, ^{232}Th and ^{238}U. U, Th and Pb concentrations were calibrated by using ^{29}Si as an internal standard and NIST SRM 610 as the reference standard. Each analysis consists of 30 s gas blank and 40 s signal acquisition. High-purity argon was used together with a custom helium filtration column, which resulted in ^{204}Hg and ^{202}Hg being less than 100 cps in the gas blank. Therefore, the contribution of ^{204}Hg to ^{204}Pb was negligible and no correction was made. $^{207}Pb/^{206}Pb$, $^{206}Pb/^{238}U$, $^{207}Pb/^{235}U$ and $^{208}Pb/^{232}Th$ ratios, calculated using GLITTER 4.0 (Macquarie University), were corrected for both instrumental mass bias and depth-dependent elemental and isotopic fractionation using Harvard zircon 91500 as the external standard. The ages were calculated using ISOPLOT 3 (Ludwig 2003). Our measurement of TEMORA 1 as an unknown yielded a weighted $^{206}Pb/^{238}U$ age of 415±4 Ma (MSWD=0.112, n=24) (Yuan et al. 2004), which is in good agreement with the recommended ID-TIMS age of 416.75±0.24 Ma (Black et al. 2003). Analytical details for age and trace and rare earth element determinations of zircons are reported in Yuan et al. (2004). Common Pb corrections were made following the method of Andersen (2002). Because measured ^{204}Pb usually accounts for <0.3 percent of the total Pb, the correction is insignificant in most cases.

$^{40}Ar/^{39}Ar$ analytical technique

$^{40}Ar/^{39}Ar$ techniques largely follow descriptions given in Handler et al. (2004) and Rieser et al. (2006). Preparation of the samples before and after irradiation, $^{40}Ar/^{39}Ar$ analyses, and age calculations were carried out at the ARGONAUT Laboratory of the Department of Geography and Geology at the University of Salzburg. The white mica concentrate was packed in aluminium-foil and placed in a quartz vial. For calculation of the J-values, flux-monitors were placed between each 4–5 unknown samples. The sealed quartz vials were irradiated in the Řež reactor (Prague, Czech Republic) for 16 hours. Correction factors for interfering isotopes were calculated from 45 analyses of two Ca-glass samples and 70 analyses of two pure K-glass samples and are: $^{36}Ar/^{37}Ar_{(Ca)}$= 0.000225, $^{39}Ar/^{37}Ar_{(Ca)}$=0.000614, $^{38}Ar/^{39}Ar_{(Ca)}$=0.011700 and $^{40}Ar/^{39}Ar_{(K)}$=0.0266. Variations in the flux of neutrons were monitored using the DRA1 sanidine standard for which an $^{40}Ar/^{39}Ar$ plateau age of 25.26±0.05 Ma is reported (van Hinsbergen et al. 2008).

$^{40}Ar/^{39}Ar$ analyses were carried out using a UHV Ar-extraction line equipped with a combined MERCHANTEKTM UV/IR laser system, and a VG-ISOTECHTM NG3600 mass spectrometer. Isotopic ratios, ages and errors for individual steps were calculated following suggestions by McDougall & Harrison (1999) and Scaillet (2000) using decay factors reported by Renne et al. (2011). Definition and calculation of plateau ages was carried out using ISOPLOT/EX (Ludwig 2003).

Results from the Reifnitz tonalite

Petrography

All investigated samples of the Reifnitz tonalite show a strong low-temperature alteration, mostly sericitization and carbonatization. The grain size of porphyric minerals ranges from 1.5 to 5 mm, whereas feldspar and subordinate interstitial quartz of the matrix are ca. 0.1 mm in size. Dominant euhedral plagioclase, subordinate K-feldspar and rare rounded quartz phenocrysts are observed. Quartz phenocrysts show resorption embayments, feldspar some garnet inclusions. Phenocrystic and matrix feldspars are heavily sericitized, transformed to sericite or clay minerals and are in part replaced by carbonate (Fig. 4a, b). In very few cases, relics of oscillatory normal zoning of plagioclase could be observed indicating andesine and oligoclase compositions. Biotite phenocrysts with a length of 0.7 to 1.5 mm are generally transformed into chlorite, leucoxene and carbonate. In places, elongated xenocrystic garnet grains in the matrix and as inclusions within feldspar are common, ranging in size from 1–2 mm, rarely up to 4 mm. Further minerals include euhedral zircons, apatite and opaque minerals. Alteration of samples was too strong to carry out geochemical investigations except for well preserved garnet.

Garnet composition

Back-scattered electron images show the zoned nature of garnet. The large garnet grains were formed by coalescence of small garnet grains preserved in the core (Fig. 5a). Several small garnet grains coalesced into an aggregate, which is surrounded by an inner and an outer rim, which represent almandine-rich garnets (Table 1; Fig. 5a,b). The growth pattern is well reflected by chemical variation of MgO, CaO and MnO contents (Table 1; Fig. 5b). The core is high in MgO (4.9 wt. %), poor in MnO (1.0 wt. %), and low in CaO content (7.9 wt. %) compared to the inner rim, which has higher MnO (2.6 wt. %), and CaO (8.4 wt. %) and lower MgO (2.5 wt. %) contents (Fig. 5b). The outer rim is low in MnO (1.5 wt. %) and CaO (5.2 wt. %), but high in MgO (4.8 wt. %). The boundaries between the three zones are diffuse (Fig. 5a). The generally high FeO and Al_2O_3 contents classify the garnet as almandine-rich garnet.

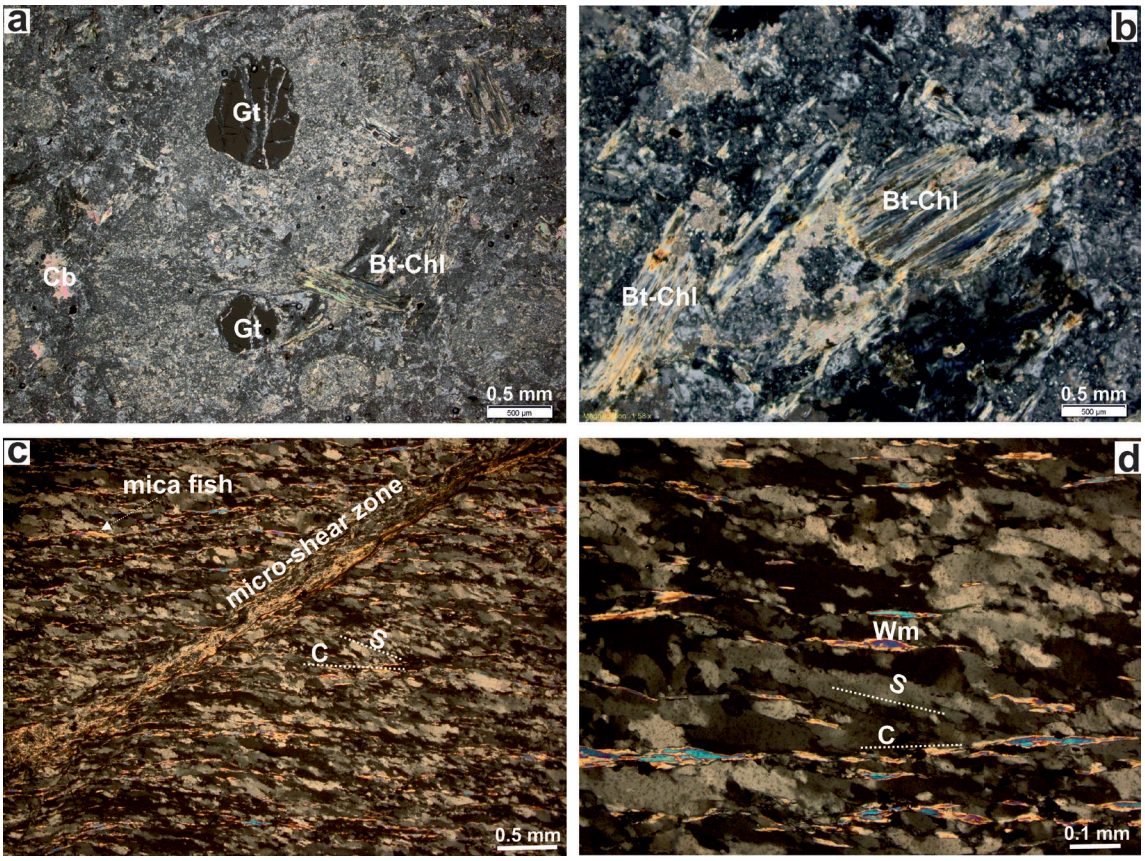

Fig. 4. a and **b** — Photomicrographs of thin sections of the Reifnitz tonalite (sample KAR-25). **a** — Garnet grains within altered feldspar phenocryst surrounded by fine-grained matrix. **b** — Chloritized biotite surrounded by a fine-grained matrix of feldspar and quartz, which includes calcite and sericite as alteration products. **c** and **d** — Mylonitic, sheared quartzite from the basement complex (sample KAR-24). Abbreviations: Bt-Chl — chloritized magmatic biotite, Cb — calcite, Gt — garnet, Wm — white mica.

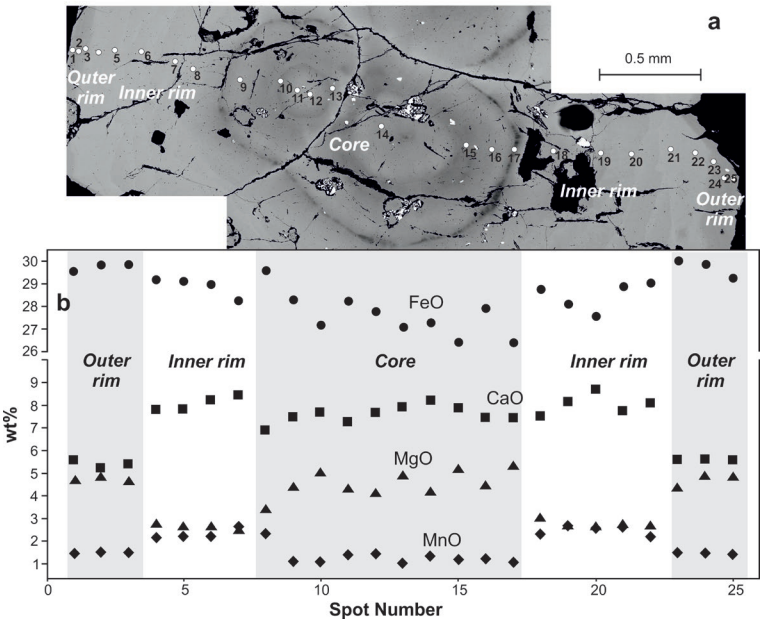

Fig. 5. Garnet composition of the Reifnitz tonalite. **a** — Back-scattered electron image of a composite garnet grain and measured points. **b** — Compositional variation along the garnet profile.

U–Pb dating results

Zircons of sample KAR-25 (46°35'48" N, 14°08'31" E) are generally euhedral. Cathodoluminescence images show either regular, sometimes complex oscillatory magmatic zoning, or zircons are internally rather uniform (Fig. 6). 30 spots have been measured on zircons of sample KAR-25 (Table 2; Figs. 6, 7). The U contents range from 532 to 2216 µg/g and the Th contents are much lower, 25 to 178 µg/g. The Th/U ratio varies between 0.025 and 0.1, which is not typical for magmatic zircons. Typical Th/U ratios in magmatic zircons are >0.1 (Hoskin & Schaltegger 2003; Kirkland et al. 2015). Most spots plot on the concordia curve; the weighted mean age of 22 spots is 30.72±0.30 Ma (MSWD=2.6). One euhedral grain (spot 12) with an oscillatory magmatic zoning at the rim and a patchy internal pattern is significantly older, with a $^{236}U/^{206}Pb$ age, 107.3±1.4 Ma, and is explained as an inherited potentially metamorphic core within that grain.

(U–Th–Sm)/He dating results

Three apatite grains from sample KAR-25 were measured. Data were included in Heberer et al. (2017) but not discussed and interpreted in detail with respect to the local geology. One grain is older (38.9±5.7 Ma) than the U–Pb zircon age. Consequently, we consider that the age result of this grain unreliable, and might have its cause in undetected inclusions of a U-rich phase. The other two grains have similar ages and the average of the two grains yields an age of 27.6±1.8 Ma (Heberer et al. 2017).

Metamorphic host rocks: microfabrics and $^{40}Ar/^{39}Ar$ white mica age

The foliation of the metamorphic host rocks is gently south-dipping and the stretching lineation trends E–W. We examined a few thin sections of the metamorphic rocks, which mainly comprise garnet-bearing micaschist and subordinate lenses of garnet-amphibolite, epidote-amphibolite and thin marble lenses, variably retrogressed by chloritization under greenschist facies metamorphic conditions. For $^{40}Ar/^{39}Ar$ white mica dating, we selected a strongly sheared quartzite

Table 1: Representative garnet composition of the three zones of the composite garnet grain graphically shown in Figure 5.

Spot	SiO_2	Al_2O_3	MgO	Na_2O	CaO	TiO_2	FeO	MnO	Cr_2O_3	K_2O	NiO	P_2O_5	O	Total
2	37.84	21.19	4.87	0.03	5.22	0.35	29.82	1.48	0.04	0.00	0.00	0.00	0.00	100.87
7	37.41	21.09	2.51	0.03	8.47	0.24	28.25	2.61	0.01	0.00	0.03	0.04	0.00	100.71
13	37.74	21.01	4.93	0.02	7.95	0.59	27.08	1.00	0.02	0.00	0.01	0.09	0.00	100.42
Spot	**Si**	**Al**	**Mg**	**Na**	**Ca**	**Ti**	**Fe**	**Mn**	**Cr**	**K**	**Ni**	**P**	**O**	**Sum**
2	5.94	3.92	1.14	0.01	0.88	0.04	3.92	0.20	0.01	0.00	0.00	0.00	24.00	40.06
7	5.94	3.94	0.59	0.01	1.44	0.03	3.75	0.35	0.00	0.00	0.00	0.01	24.00	40.06
13	5.92	3.88	1.15	0.01	1.33	0.07	3.55	0.13	0.00	0.00	0.00	0.01	24.00	40.06

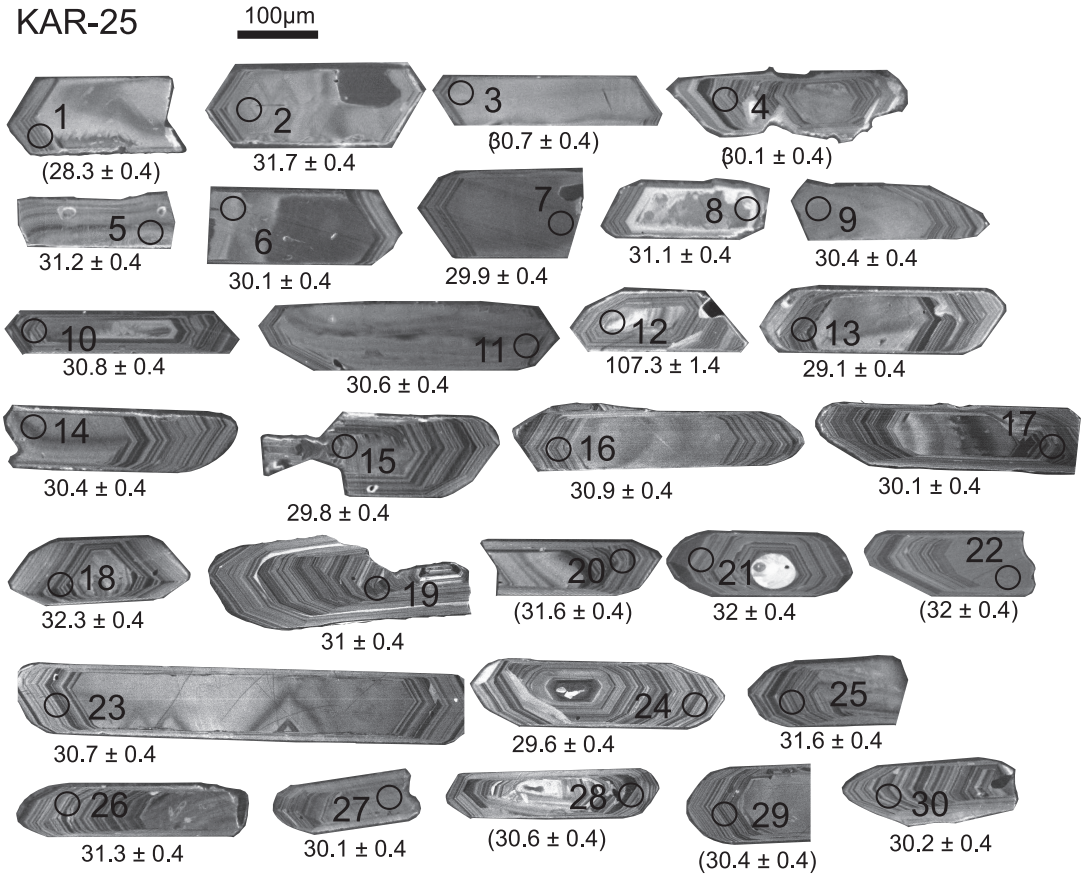

Fig. 6. Cathodoluminescence images of dated zircons. $^{238}U/^{206}Pb$ ages are given. Ages in brackets are discordant outside of 90–110 percent.

Table 2: U–Pb zircon analytical data of the Reifnitz tonalite (sample KAR-25).

Spot #	Isotope ratios								Ages									
	Pb^{207}/Pb^{206}	1s	Pb^{207}/U^{235}	1s	Pb^{206}/U^{238}	1s	Pb^{208}/Th^{232}	1s	Pb^{207}/Pb^{206}	1s	Pb^{207}/U^{235}	1s	Pb^{206}/U^{238}	1s	Pb^{208}/Th^{232}	1s	concordia	Th/U
1	0.084	0.00338	0.051	0.00148	0.00441	0.00007	0.01466	0.00041	1292	76.5	50.5	1.4	28.3	0.43	294.3	8.2	178.4	0.03
2	0.0471	0.00159	0.03196	0.00065	0.00492	0.00007	0.0019	0.00004	54.3	79	31.9	0.6	31.7	0.43	38.4	0.9	100.6	0.07
3	0.0533	0.00193	0.03507	0.00084	0.00478	0.00007	0.00217	0.00006	341.2	79.96	35.0	0.8	30.7	0.43	43.8	1.2	114.0	0.08
4	0.0503	0.00178	0.03371	0.00077	0.00487	0.00007	0.00151	0.00005	206.5	80.04	33.7	0.8	31.3	0.43	30.4	1	107.7	0.05
5	0.0453	0.00152	0.03025	0.00061	0.00485	0.00007	0.00151	0.00005	0.1	37.3	30.3	0.6	31.2	0.42	30.5	1	97.1	0.04
6	0.0503	0.00214	0.03241	0.00105	0.00468	0.00007	0.00194	0.0001	207.2	95.67	32.4	1	30.1	0.44	39.2	2	107.6	0.05
7	0.0474	0.00169	0.03035	0.0007	0.00464	0.00006	0.00167	0.00006	70.5	83.28	30.4	0.7	29.9	0.41	33.8	1.3	101.7	0.04
8	0.0458	0.00161	0.03054	0.00069	0.00484	0.00007	0.00148	0.00004	0.1	70.7	30.5	0.7	31.1	0.42	29.9	0.9	98.1	0.07
9	0.0477	0.00169	0.03111	0.00071	0.00473	0.00007	0.0022	0.00007	84.6	82.8	31.1	0.7	30.4	0.42	44.4	1.3	102.3	0.05
10	0.0458	0.0015	0.03028	0.00057	0.0048	0.00006	0.00169	0.00003	0.1	64.75	30.3	0.6	30.8	0.42	34.2	0.7	98.4	0.09
11	0.0472	0.00158	0.03095	0.00062	0.00476	0.00006	0.00173	0.00004	59.5	78.58	30.9	0.6	30.6	0.42	35.0	0.8	101.0	0.07
12	0.0523	0.00171	0.12096	0.00225	0.01678	0.00023	0.00278	0.00008	299.5	72.73	115.9	2	107.3	1.44	56.1	1.5	108.0	0.10
13	0.0494	0.00174	0.03078	0.0007	0.00452	0.00006	0.0014	0.00004	166.3	80.5	30.8	0.7	29.1	0.4	28.4	0.8	105.8	0.08
14	0.0454	0.00149	0.02954	0.00056	0.00472	0.00006	0.00141	0.00003	0.1	44.41	29.6	0.6	30.4	0.41	28.5	0.5	97.4	0.15
15	0.046	0.0015	0.02939	0.00055	0.00463	0.00006	0.00136	0.00003	0.1	75.48	29.4	0.5	29.8	0.4	27.5	0.6	98.7	0.06
16	0.0453	0.00159	0.02993	0.00067	0.0048	0.00007	0.00167	0.00005	0.1	40.66	29.9	0.7	30.9	0.43	33.7	1	96.8	0.06
17	0.0492	0.00159	0.03171	0.00057	0.00468	0.00006	0.00257	0.00006	155.6	73.81	31.7	0.6	30.1	0.41	51.9	1.1	105.3	0.04
18	0.0554	0.00205	0.03838	0.00097	0.00503	0.00007	0.00366	0.00012	429.4	80.4	38.2	1	32.3	0.46	73.9	2.3	118.3	0.04
19	0.0461	0.00165	0.03062	0.00072	0.00482	0.00007	0.00173	0.00007	3.4	83.06	30.6	0.7	31.0	0.43	34.9	1.3	98.7	0.04
20	0.0464	0.0016	0.03139	0.00068	0.00491	0.00007	0.0016	0.00004	17.1	79.61	31.4	0.7	31.6	0.44	32.2	0.8	99.4	0.09
21	0.0461	0.00155	0.03153	0.00064	0.00497	0.00007	0.00179	0.00004	0.1	78.99	31.5	0.6	32.0	0.44	36.2	0.9	98.4	0.07
22	0.0372	0.00132	0.02551	0.0006	0.00498	0.00007	0.00169	0.00004	0.1	0	25.6	0.6	32.0	0.44	34.1	0.7	80.0	0.08
23	0.0462	0.00161	0.03043	0.00067	0.00478	0.00007	0.00169	0.00004	7.7	80.82	30.4	0.7	30.7	0.43	34.1	0.8	99.0	0.09
24	0.0478	0.00179	0.03033	0.00079	0.0046	0.00007	0.00197	0.00007	89.8	87.47	30.3	0.8	29.6	0.42	39.8	1.4	102.4	0.06
25	0.0471	0.00161	0.0319	0.00067	0.00492	0.00007	0.00159	0.00004	53.2	79.83	31.9	0.7	31.6	0.44	32.2	0.9	100.9	0.07
26	0.0453	0.00156	0.03046	0.00066	0.00487	0.00007	0.00172	0.00004	0.1	43.7	30.5	0.7	31.3	0.44	34.7	0.9	97.4	0.08
27	0.0511	0.00173	0.03292	0.00069	0.00468	0.00007	0.00201	0.00005	243.5	76.37	32.9	0.7	30.1	0.42	40.6	1	109.3	0.06
28	0.0557	0.00183	0.03658	0.0007	0.00476	0.00007	0.00243	0.00005	441.6	71.35	36.5	0.7	30.6	0.42	49.1	0.9	119.3	0.10
29	0.0514	0.00168	0.03354	0.00064	0.00473	0.00007	0.00198	0.00004	259.4	73.52	33.5	0.6	30.4	0.42	40.0	0.8	110.2	0.08
30	0.0475	0.00156	0.03074	0.00059	0.0047	0.00007	0.00149	0.00005	71.9	77.21	30.7	0.6	30.2	0.42	30.0	0.9	101.7	0.04

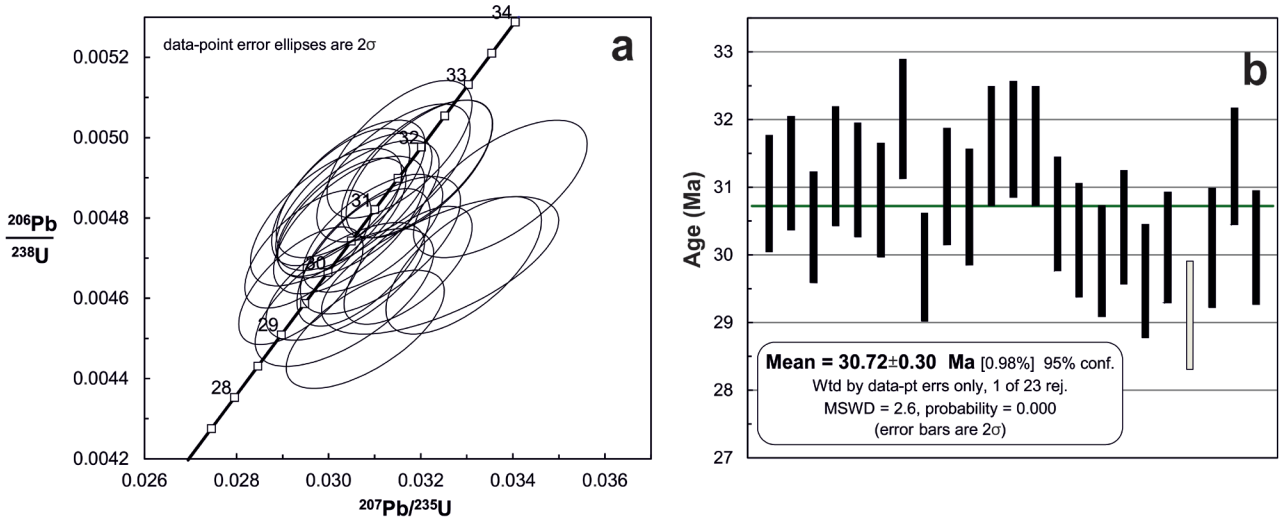

Fig. 7. a — U–Pb zircon concordia age plot of the Reifnitz tonalite, sample KAR-25. **b** — Weighted mean age.

(sample KAR-24; 46°36'33" N, 14°08'52" E) with a ca. E–W trending stretching lineation, showing S–C fabrics and shear bands (Fig. 4c, d). The S-foliation is formed by strongly elongated quartz grains, showing a shape preferred orientation, whereas the C-foliation is formed by white mica (Fig. 4c,d). In this peculiar case, the shear is top to the west. Grain boundaries of quartz show bulging, which is typical for temperatures lower than ca. 400 °C (Stipp et al. 2002). Small white mica occurs as mica-fish with a grain-size of 0.05 to 0.2 mm. Further minerals are abundant zircon and rare apatite decorated by fine opaque minerals. The ductile S–C fabric is sometimes overprinted or cut at high angle by small semiductile to cataclastic micro-shear zones (Fig. 4c), which deflect the earlier S–C fabric. The micro-shear zones consist mainly of fine-grained quartz and sericite.

We selected white mica (grain size fraction of 125–200 µm) for $^{40}Ar/^{39}Ar$ analysis from an orthoquartzite (Table 3 for results). In the resulting Argon release pattern (Fig. 8), individual steps 1 to 8 scatter around 80 to 100 Ma and have a large individual error, whereas steps 9 to 13 show a plateau age of 90.7±1.6 Ma comprising 69.5 percent of ^{39}Ar released.

Discussion

Distribution of Upper Eocene to Oligocene magmatism along the Periadriatic fault

The new data indicate that the Reifnitz tonalite belongs to the Eocene–Oligocene Periadriatic plutons. It represents one of the northernmost plutonic bodies, relatively distant from the Periadriatic fault. It also represents the easternmost Oligocene Periadriatic pluton north of the Periadriatic fault. Major plutons north of the Periadriatic fault are the Biella, Bergell (Oberli et al. 2004; Rosenberg 2004) and Rieserferner (Romer & Siegesmund 2003; Wagner et al. 2006)). However, many younger dykes (20–14 Ma) are present, which stretch from the Kreuzeck Mts. (Deutsch 1980, 1984) and may be correlative, as a zone, with volcanics and volcanic necks in the Lavant Valley area (Kollnitz in Fig. 2; Lippolt et al. 1975) and in the Styrian basin (Ebner & Sachsenhofer 1995; Handler et al. 2006). The Pohorje pluton with its age of ca. 18 Ma is the only major pluton of that zone (Fodor et al. 2008; Trajanova et al. 2008).

The distribution of (1) Upper Eocene to Oligocene plutons and rare volcanics (Smrekovec) (42–28 Ma) and the younger Miocene (20–14 Ma) plutons and volcanics is quite interesting and shows a hitherto unexplained phenomenon (Fig. 1; Rosenberg 2004). In the western PP segment (to the west of the Adamello pluton; Fig. 1), Oligocene magmatic rocks including dykes are widespread both in the Southalpine unit as well as in Austroalpine units. In the central PP segment, the Adamello (42–30 Ma; Brack 1983; Schoene et al. 2012; Bergomi et al. 2015) and Bergell plutons and associated dykes indicate the largest N–S-extent of Periadriatic plutons across the Periadriatic fault dominated by the huge Adamello body and many dykes. In the eastern PP segment, plutons and dykes are only present along and north of the Periadriatic fault (e.g., Pomella et al. 2011, 2012). This distribution cannot be explained by a simple slab break-off model alone, which would imply an along strike-strike younging of magmatism (Wortel & Spakman 2000) according to the lateral progression of the slab window. The oldest pluton (Adamello with an age extending from 42 to 30 Ma) occurs in the central segment and its age distribution shows that the Oligocene magmatic rocks occur south of the Periadriatic fault in the western segment, in the eastern segment to the north. This feature could be tentatively explained by initiation of magmatism in the central segment and potential post-30 Ma dextral displacement of the segments north of and shearing along the Periadriatic fault. The eastern segment is then overprinted by Miocene magmatism (Fig. 1), which seems to be independent of Oligocene

Table 3: $^{40}Ar/^{39}Ar$ analytical data of a white mica concentrate from a mylonitic quartzite from the basement (sample KAR-24).

Sample: KAR-24	Mu	125–200 µm	12 grains	J-Value: 0.010717± 0.000046												
step	^{36}Ar meas.	$\pm\sigma_{36}$	^{37}Ar decay corr.	$\pm\sigma_{37}$	^{38}Ar meas.	$\pm\sigma_{38}$	^{39}Ar decay corr.	$\pm\sigma_{39}$	^{40}Ar meas.	$\pm\sigma_{40}$	$^{40}Ar^*/^{39}Ar_K$	± σ	$\%^{40}Ar^*$	$\%^{39}Ar$	age [Ma]	± [Ma] 1σ abs.
1	2.5874E+00	7.60E+00	3.9627E+01	5.32E+01	1.2555E+01	1.88E+01	1.8263E+03	8.72E+01	1.0795E+04	2.84E+01	5.49	1.26	92.9	0.9	103.2	23.0
2	9.5487E+00	7.31E+00	3.5671E+01	3.11E+01	4.0759E+01	1.88E+01	3.6736E+03	5.95E+01	2.0306E+04	5.06E+01	4.76	0.59	86.1	1.8	89.7	10.9
3	3.6454E-01	1.14E+01	4.4321E+01	5.32E+01	8.7755E+01	1.50E+01	4.6279E+03	5.40E+01	3.0453E+04	7.58E+01	6.56	0.73	99.6	2.2	122.5	13.2
4	1.6586E+01	1.11E+01	2.3902E+00	5.73E+01	1.1508E+02	9.87E+00	8.7171E+03	3.33E+01	6.0623E+04	1.14E+02	6.39	0.38	91.9	4.2	119.5	6.8
5	1.7896E+01	1.16E+01	8.3173E+01	5.14E+01	1.5759E+02	1.47E+01	9.6721E+03	3.28E+01	5.7560E+04	6.29E+01	5.40	0.35	90.8	4.7	101.6	6.5
6	1.8696E+01	1.22E+01	2.4501E+00	5.54E+01	2.2282E+02	1.94E+01	1.3947E+04	4.11E+01	7.5686E+04	4.01E+01	5.03	0.26	92.7	6.8	94.7	4.8
7	8.7185E+00	1.32E+01	1.2889E+02	4.43E+01	2.3618E+02	1.62E+01	1.8841E+04	5.81E+01	1.0096E+05	1.11E+02	5.22	0.21	97.4	9.1	98.2	3.8
8	1.7717E+01	8.73E+00	8.0799E+01	6.25E+01	4.0913E+02	2.35E+01	2.9660E+04	5.86E+01	1.5016E+05	1.31E+02	4.88	0.09	96.5	14.4	92.1	1.7
9	2.0966E+01	1.05E+01	1.6429E+01	4.09E+01	4.3093E+02	2.12E+01	3.4327E+04	5.69E+01	1.7312E+05	1.19E+02	4.86	0.09	96.4	16.6	91.6	1.7
10	1.8873E+01	1.03E+01	8.4137E+01	4.61E+01	5.0616E+02	2.72E+01	3.9788E+04	5.51E+01	1.9501E+05	1.34E+02	4.76	0.08	97.1	19.3	89.8	1.5
11	6.2432E+01	1.06E+01	4.9194E+01	4.92E+01	4.0075E+02	2.44E+01	3.1794E+04	5.50E+01	1.6823E+05	1.01E+02	4.71	0.10	89.0	15.4	88.8	1.8
12	7.9445E+01	1.29E+01	6.1102E+00	4.60E+01	1.0147E+02	1.70E+01	7.9311E+03	5.56E+01	6.7367E+04	5.99E+01	5.53	0.48	65.1	3.8	103.9	8.8

magmatism and was either related to the polarity reversal of the subduction zone (Lippitsch et al. 2003; Handy et al. 2015) or with a second stage of post-collisional slab break-off magmatism starting in the south-eastern Alps and progressing along the Carpathian arc (Wortel & Spakman 2000).

Significance of garnet in the tonalite

A peculiar feature is the occurrence of garnet in the Reifnitz tonalite, which is typical for S-type granites and rare but present in some I-type granitoids(e.g., Pe-Piper 2000; Harangi et al. 2001; Samadi et al. 2014 and references therein). René & Stelling (2007) summarized potential models for the occurrence of garnet in granitoids, which is more common in S-type granitoids and rare in I-type granitoids (see also Harangi et al. 2001): (1) garnet could represent a refractory restite phase transported within the magma from the area of partial melting, or (2) a refractory xenocryst phase from high-grade metasedimentary country rocks, or (3) could have crystallized in the marginal facies of a granitic intrusion as a result of reaction between granitic melt and pelitic xenoliths rich in Al and Mn compared to the melt. Because of strong alteration particularly of feldspars in the investigated samples, no equilibrium of garnet and plagioclase or biotite could be observed, which would allow us to estimate the P–T conditions of garnet crystallization at depth. However, because of the high CaO content of ca. 8 percent in core and inner rim we can conclude that the almandine-rich garnet cores likely represents either refractory xenocrysts incorporated at lower/middle levels of the crust into the magma or represent garnet grown in a magma. These garnet aggregates likely interacted with magma forming the outer rim with a CaO content of ca. 5 percent implying crystallization at middle crustal level. The almandine-rich garnet outer rim composition with ca. 5 percent CaO is very similar to magmatic garnet, which crystallized in an I-type

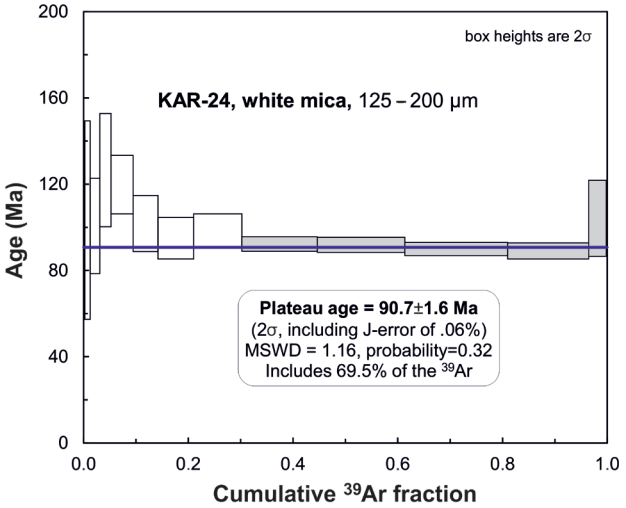

Fig. 8. $^{40}Ar/^{39}Ar$ release pattern of white mica separated from a mylonitic quartzite, sample KAR-24. Laser energy increases from left to right until fusion.

granite in Iran (Samadi et al. 2014). The CaO content requires an elevated pressure of garnet crystallization corresponding to middle to lower crustal depth (Harangi et all. 2001). However, for final clarification, more detailed investigations on less altered samples are needed, and are planned in the near future.

Similar garnets were also found in Miocene andesites of the Western Carpathians (Harangi et al. 2001; Pécskay et al. 2006; Kohút & Danišík 2017 and references therein). These garnets show a wide variation in composition and include both xenocrystic garnet, similar in composition to those in the Reifnitz tonalite, and garnets formed by growth in a deep-seated magma chamber (Harangi et al. 2001).

Implications for Cretaceous tectonics

We interpret that the $^{40}Ar/^{39}Ar$ white mica plateau age of 90.7±1.6 Ma is geologically significant and dates either (1) the age of regional cooling through ca. 425±25 °C (Harrison et al. 2009) after epidote-amphibolite facies metamorphic conditions or the last stage of ductile deformation. Besides regional cooling many other factors like hydrous fluids and deformation are influencing the resetting of the Ar isotopic system (e.g., Villa et al. 2014; Villa 2016). Thin section observations indicate that white mica is fully recrystallized during deformation. Deformation and associated fluid could have led to complete isotopic resetting as shown by the well defined plateau age.

Our findings of a Cretaceous age of metamorphism have several tectonic implications for the south-eastern Alps: The new $^{40}Ar/^{39}Ar$ age 90.7±1.6 Ma of the strongly deformed white mica of the quartzite indicates pervasive metamorphic overprint of the micaschist and intercalated quartzite with temperatures exceeding 425 °C (Ar retention temperature of white mica; Harrison et al. 2009). It seems to be likely that the micaschist reached Early Cretaceous epidote amphibolite facies metamorphic conditions as the pelitic rocks commonly include oligoclase as the main feldspar (Schwaighofer 1965 and own observations) and rare epidote-amphibolite lenses. The new $^{40}Ar/^{39}Ar$ white mica age in combination with previous data on the low-grade metamorphic overprint on Permian and Triassic cover rocks of Viktring and Rossegg Permo–Mesozoic units (Schünemann et al. 1982; von Gosen et al. 1987; von Gosen 1989) indicate pervasive metamorphic overprint of rocks within the Klagenfurt half-window, which is also supported by a Rb–Sr mica age of 84±3 Ma in the Villach orthogneiss (Göd 1976). The southern limit of Alpine metamorphism of Cretaceous age (SAM) is outlined in Fig. 2 and is located much further to the south as reported by Hoinkes et al. (1999). This also implies that there is not enough space north of the North Karawanken thrust sheet (Fig. 2) for a potential root zone of the Gurktal nappe complex, which was formed at around the Early to Late Cretaceous boundary. The Gurktal nappe complex is only the southernmost part of the Upper Austroalpine nappe complex (e.g., Neubauer 1987 and references therein). This fact indicates that the potential root zone of the Gurktal nappe complex is either displaced by Eocene to Oligocene strike-slip faults like the Periadriatic fault or subducted during Cretaceous times. This is in agreement with the area further east, where the ultra-high pressure metamorphic rocks with a Cretaceous age of the southernmost Pohorje Mts. are also juxtaposed to very low-grade- or non-metamorphic rocks of the Southalpine units (e.g., Placer 2009; Janák et al. 2016; Sandmann et al. 2016). The Pohorje area exposes the Early to Middle Miocene Pohorje pluton intruded into metamorphic rocks of Cretaceous age and thermally overprinted during Miocene times (Fodor et al. 2008) as well as the area adjacent to the north (Sachsenhofer et al. 1998). Both units were exhumed by Miocene ca. E–W extension (Fodor et al. 2008). However, the Miocene thermal overprint did not destroy the nappe structure of Cretaceous age. In summary, the root zone of the Gurktal nappe complex and other Upper Austroalpine tectonic elements is missing and likely displaced by the Periadriatic strike-slip fault.

Implications for Oligocene and Neogene tectonics of the Eastern Alps

The small occurrences of the Reifnitz tonalite are aligned in an E–W direction and the entirely crystalline fabric with relatively large porphyric grains (2–4 mm) show that the Reifnitz tonalite intruded at some depth into the basement. The exact intrusion depth is difficult to determine in the absence of well-preserved magmatic mineral assemblages. The scattered occurrences extending over about eight kilometres in an E–W direction might also indicate that the Reifnitz tonalite belongs to the plumbing system underneath a surface volcano and might represent part of a major pluton, which widens at depth (Fig. 9a as shown in an illustrative model). This interpretation of the tentative relationships between surface and depth are shown in Figs. 9 and 10.

The present-day erosional level of the "Altkristallin" basement implies denudation and erosion of at least one or two kilometres of overburden after intrusion of the Reifnitz tonalite. The Reifnitz tonalite is located in the centre of the Wörthersee antiform (Figs. 2 and 11). Here, we note that both in the northern and southern sectors of this antiform Cenozoic sedimentary units crop out. In the north, in the Krappfeld area (Fig. 2), discontinuous sedimentary successions including Upper Cretaceous, Eocene, possible Oligocene, then Lower Miocene (Karpatian) strata (e.g., Thiedig 1970, 1975; Thiedig et al. 1999) are exposed in a synform (Figs. 2, 10, 11). In the Krappfeld area, these sedimentary units are separated by angular unconformities and/or sedimentary hiatuses (Thiedig 1975; Thiedig et al. 1999). The presence of sediments implies that this segment of the Upper Austroalpine units has always been in a near-surface position since Late Cretaceous times. The presence of potentially Oligocene sediments (Appold et al. 1986) implies that this area was subsiding at the same time as the Wörthersee antiform was uprising and the Reifnitz tonalitre was cooling. For the Krappfeld area, Neubauer & Heberer (2011) proposed an Oligocene age of gentle folding predating Karpatian sediment deposition of

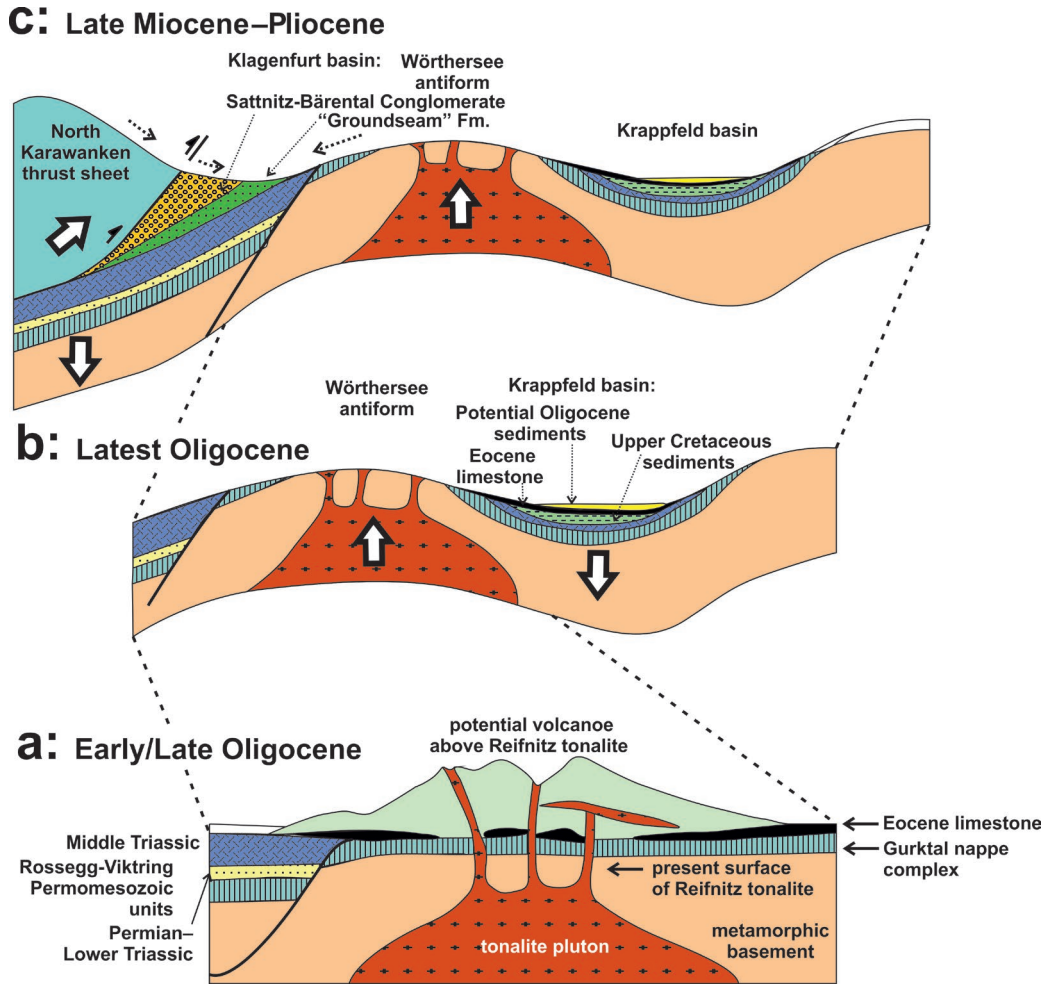

Fig. 9. Three-stage tectonic model for the evolution of the Wörthersee area in southeastern Austria. **a** — Time of intrusion of the Reifnitz tonalite with a potential volcanoe above it. **b** — Oligocene gentle folding and formation of antiforms and synforms. **c** — Formation of the peripheral bulge by flexuring the crust in front the North Karawanken thrust (after Nemes et al. 1997) and erosion of the Wörthersee antiform. White arrows indicate dominant vertical motion at the given time interval.

the Waitschach Gravel (Figs. 9b and 10), deformation D1 in Figure 9b. Together, the new data from the Wörthersee antiform indicate that the entire south-eastern Alps were affected by gentle folding due to N–S shortening (Fig. 11). Such late-stage folds were already postulated by Fritsch (1965) and Neubauer et al. (2000) assigning a loosely constrained Cenozoic age. This folding obviously affected major portions of the Austroalpine nappe complex east of the Tauern window (Fig. 2). The N–S D1 shortening was followed by Early Miocene (Karpatian?) WSW–ESE extension in the Krappfeld basin area, formation of halfgraben related to eastward lateral extrusion (Ratschbacher et al. 1989; Neubauer & Heberer 2011; deformation stage D2 in Figure 10).

South of the Reifnitz tonalite, the Sarmatian to Pliocene and possibly Quaternary infill of the Klagenfurt basin is exposed (Fig. 2) (Polinski & Eisbacher 1992; Nemes et al. 1997). This basin was interpreted to represent a flexural basin formed at the front of the N-directed Karawanken thrust (Nemes et al. 1997). This thrust is part of a major positive flower structure along the Periadriatic fault (Polinski & Eisbacher 1992; Nemes et al. 1997). Structural relationships between the Middle Miocene–Pliocene Klagenfurt basin and the Wörthersee antiform (Fig. 9c) imply that the Reifnitz tonalite is located on the peripheral bulge in the front of the flexural Klagenfurt basin. This also implies N–S to NW–SE shortening (deformation stage D3 in Figure 10), some surface uplift in front of the Klagenfurt basin in the order of several 100 m as the lithosphere underneath had a low strength (Nemes et al. 1997). Dunkl et al. (2005) reported two detrital apatite fission track age populations of (1) 30±1 Ma (or 36±14 Ma in another sample) and (2) 20±4 Ma from two sandstone samples from different locations in the Klagenfurt basin (Unterbergen and Ferlach, see Fig. 2 for locations). One of these samples contains euhedral apatites suggesting a potentially magmatic origin of grains with the age of 30±1 Ma (Dunkl et al. 2005) similar to suspected ages of volcanic material above the Reifnitz tonalite. This age group (30±1 Ma resp. 36±14 Ma) is also consistent with the (U–Th–Sm)He apatite

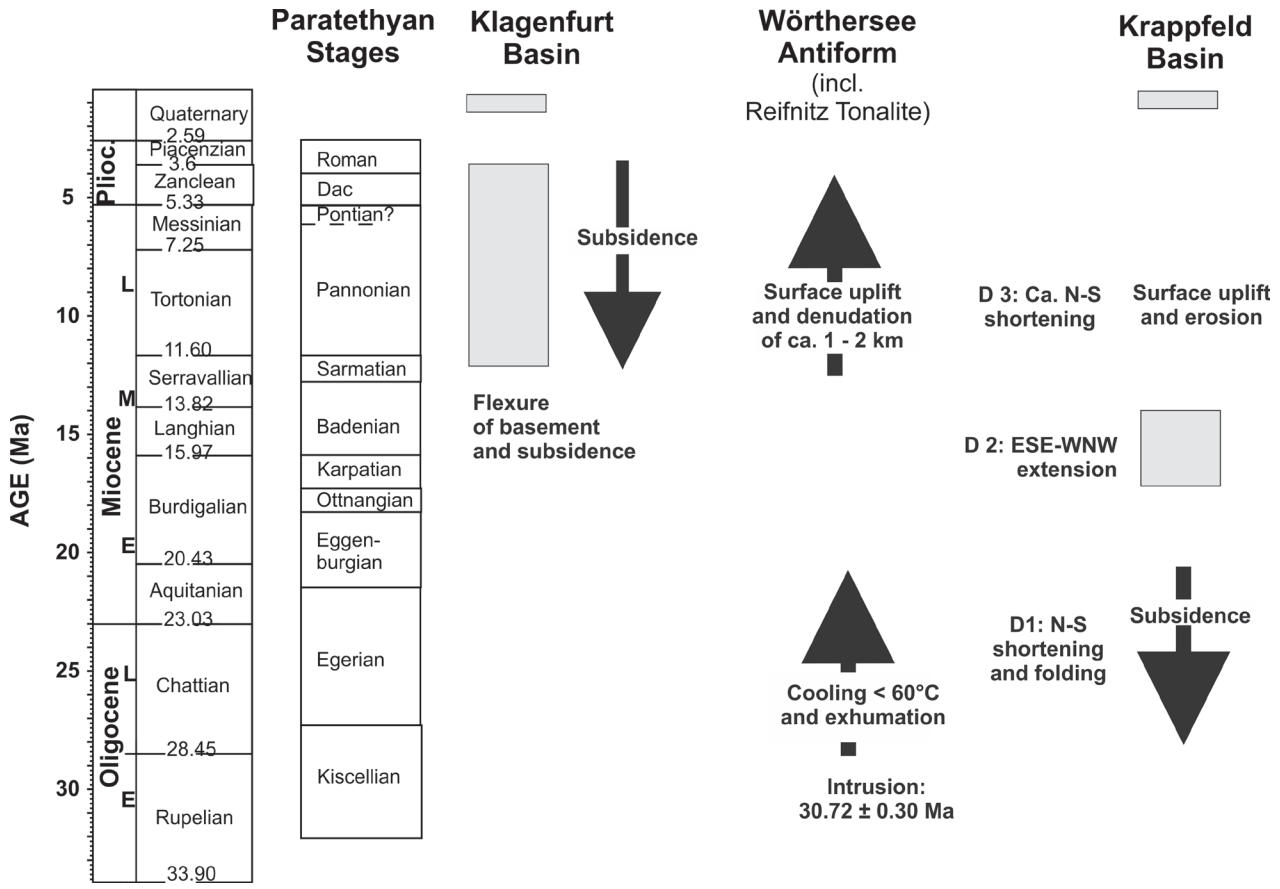

Fig. 10. Schematic diagram showing the relationships between the Oligocene Wörthersee anticline, which also corresponds to the peripheral bulge of Neogene Klagenfurt basin, and the adjacent Cenozoic sedimentary basins in southeastern Alps. Time scale after Ogg et al. (2008) and Piller et al. (2007). Note that the exact onset and termination of the three mentioned deformation stages are uncertain because of the poorly dated sedimentary rocks.

age of the Reifnitz tonalite and with the apatite fission track age of 29.8±2.1 Ma from the Villach orthogneiss (Hejl 1997, 1999; Fig. 2). The latter is also located on the Wörthersee antiform within the Klagenfurt half-window.

Kahler & Papp (1968) report many Eocene limestone pebbles in the Sattnitz conglomerate and even in the Quaternary Drau River sediments. Most of them have a close affinity to Eocene limestones now exposed at the northern margin of the Krappfeld basin (Kahler & Papp 1968). In the present drainage basin of the Drau no such limestones are exposed. The presence of such Eocene limestones could be taken as evidence, that the Eocene cover was much more widespread between Sattnitz and Krappfeld and could have been potentially eroded since late Middle Miocene (Fig. 9c).

Our new data imply, therefore, that the Reifnitz tonalite is part of a combined post-30 Ma antiform and peripheral bulge (Figs. 9c, 10 and 11). In a first step, which is dated as ca. 31–27 Ma, rapid cooling to ca. 60 °C and exhumation of the Reifnitz tonalite occurred in an E–W trending antiform, which formed as a result of regional compression that also affected the Krappfeld area further north (Neubauer & Heberer 2011). In a second, Sarmatian–Pliocene step, final exhumation of several 100 metres occurred in response to the lithospheric flexure in front of the overriding North Karawanken thrust sheet (Fig. 9c).

This later stage of deformation, Late Miocene to Pliocene in age, coincides with approximately N–S shortening in the eastern Alps, the Slovenian Sava fold (Fodor et al. 2002) region and the wider Pannonian basin area (Fodor et al. 1998, 2002; Kiss & Fodor 2007).

Conclusions

The new data from the hitherto undated Reifnitz tonalite and its metamorphic host rocks suggest the following conclusions:

- The "Altkristallin" basement complex south of the Wörthersee was fully affected by metamorphism of Cretaceous age.
- The laser ICP-MS U–Pb zircon age of the Reifnitz tonalite is 30.72±0.30 Ma and the tonalite intruded into the likely epidote amphibolite-grade metamorphic Austroalpine basement of Cretaceous age ($^{40}Ar/^{39}Ar$ white mica: 90.7±1.6 Ma) south of the Wörthersee area.

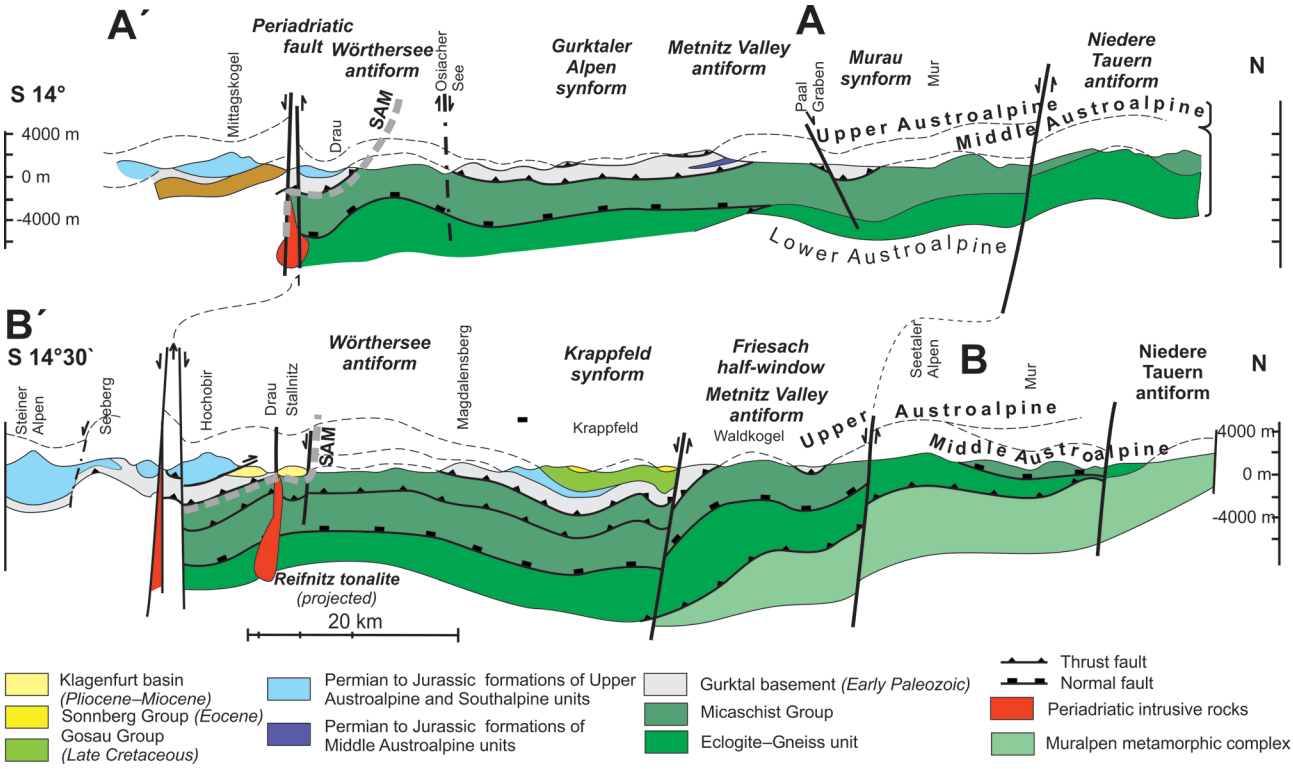

Fig. 11. Simplified structural sections showing large-scale folds in southeastern sectors of Eastern Alps (strongly modified after Fritsch 1965, who mentioned, for the first time, these undated gentle folds). The nomenclature of folds is largely from Fritsch (1965). For locations of sections, see Figure 2. SAM — Southern limit of Alpine metamorphism.

- The (U–Th–Sm)/He apatite age of the tonalite is 27.6±1.8 Ma indicates fast cooling and rapid exhumation after intrusion. The intrusion occurred into a large-scale antiformal structure, which initially formed during Late Oligocene times.
- In a second step, during the Sarmatian–Pliocene time interval, final exhumation of several hundred metres occurred in response to lithospheric flexure in front of the overriding North Karawanken thrust sheet, responsible for formation of the peripheral bulge in the front of the Klagenfurt basin.

Acknowledgements: We acknowledge valuable comments and suggestions by László Fodor and an anonymous reviewer, the topical editor Jaroslav Lexa, and the managing editor, Milan Kohút. These helped to clarify ideas and presentation. The final work has been done within the framework of project P22110 of the Austrian Science Fund FWF.

References

Andersen T. 2002: Correction of common lead in U–Pb analyses that do not report ^{204}Pb. *Chem.Geol. 192,* 59–79.

Appold T. & Pesch P. 1984: Die Tektonik der postvariskischen Transgressionsserie im Krappfeld (Kärnten/Österreich). *Carinthia II* 174, 94, 319–337.

Appold T., Thiedig F., Vollmer T. & Wilkens E. 1986: Ein neues Alttertiärvorkommen am Dachberg südlich Guttaring/Kärnten (Österreich). *Carinthia II* 176, 96, 303–310.

Bergomi M.A., Zanchetta S. & Tunesi A. 2015: The Tertiary dike magmatism in the Southern Alps: geochronological data and geodynamic significance. *Int. J. Earth Sci. (Geol. Rundsch.)* 104, 449–473.

Bigi G., Cosentino M., Parotto R., Sartori R. & Scandone P. (Eds.) 1990: Structural Model of Italy, 1:500,000, Sheets No. 1 & 2. *Consiglio Nazionale delle Ricerche*, Firenze.

Black L.P., Kamo S.L., Allen C.M., Aleinikoff J.N., Davis D.W., Korsch R.J. & Foudoulis C. 2003: TEMORA 1: A new zircon standard for Phanerozoic U–Pb geochronology. *Chem. Geol.* 200, 155–170.

Brack P. 1983: Multiple intrusions — Examples from the Adamello batholith (Italy) and their significance on the mechanisms of intrusion. *Mem. Soc. Geol. Ital.* 26, 145–157.

Brown M. 2013: Granite: From genesis to emplacement. *Geol. Soc. Amer. Bull.* 125, 1079–1113.

Cao S. & Neubauer F. 2016: Deep crustal expressions of exhumed strike-slip fault systems: Shear zone initiation on rheological boundaries. *Earth Sci. Rev.* 162, 155–176,

Claasen T., von Gosen W. , Sylvester H. & Thiedig F. 1987: Die Permotrias und ihr Grundgebirge zwischen Faaker See und Turiawald südöstlich von Villach (Kärnten/Österreich). *Jahrb. Geol. Bundesanst.* 130, 391–413.

D'Adda P., Zanchi A., Bergomi M., Berra F., Malusà M.G., Tunesi A. & Zanchetta S. 2011: Polyphase thrusting and dyke emplacement in the central Southern Alps. *Int. J. Earth Sci. (Geol. Rundsch.* 100, 1095–1113.

Dachs E. 2004: PET: Petrological Elementary Tools for Mathematica (R): an update. *Computers & Geosciences* 30, 173–182.

Dal Piaz G.B., Del Moro A., Martin S. & Venturelli G. 1988: Post-collisional magmatism in the Ortler-Cevedale Massif (Northern Italy*). Jahrb. Geol. Bundesanst.* 131, 533–551.

Davies J. H. & von Blanckenburg F. 1995: Slab breakoff: A model of lithosphere detachment and its test in the magmatism and deformation of collisional orogens. *Earth Planet. Sci. Lett.* 129, 85–102.

Deutsch A. 1980: Alkalibasaltische Ganggesteine aus der westlichen Goldeckgruppe (Kärnten/Österreich). *Tschermaks Mineral. Petrogr. Mitt.* 27, 17–34.

Deutsch A. 1984: Young Alpine dykes south of the Tauern Window (Austria): a K–Ar and Sr isotope study. *Contrib. Mineral. Petrol.* 85, 1, 45–57.

Dunkl I., Kuhlemann J., Reinecker J. & Frisch W. 2005: Cenozoic relief evolution of the Eastern Alps — constraints from apatite fission track age-provenance of Neogene intramontane sediments. *Austrian J. Earth Sci.* 98, 92–105.

Ebner F. & Sachsenhofer R.F. 1995: Paleogeography, subsidence and thermal history of the Neogene Styrian Basin (Pannonian Basin system, Austria). *Tectonophysics* 242, 133–150.

Farley K.A., Wolf R.A. & Silver L.T. 1996: The effects of long alpha-stopping distances on (U–Th)/He ages. *Geochim. Cosmochim. Acta* 60, 4223–4229.

Fodor L., Jelen B., Márton E., Skaberne D., Car J. & Vrabec M. 1998: Miocene–Pliocene tectonic evolution of the Slovenian Periadriatic fault: Implications for Alpine-Carpathian extrusion models. *Tectonics* 17, 690–709.

Fodor L., Jelen B., Márton E., Rifelj H., Kraljić M., Kevrić R., Márton P., Koroknai B. & Báldi-Beke M. 2002: Miocene to Quaternary deformation, stratigraphy and paleogeography in Northeastern Slovenia and Southwestern Hungary. *Geologija* 45, 103–114.

Fodor L., Gerdes A., Dunkl I., Koroknai B., Pécskay Z., Trajanova M., Horváth P., Vrabec M., Balogh K., Jelen B. & Frisch W. 2008: Miocene emplacement and rapid cooling of the Pohorje pluton at the Alpine–Pannonian–Dinaric junction: a Geochronological and structural study. *Swiss J. Geosci.* 101, Supplement 1, S255–S271.

Fritsch W. 1965: Das Kristallin von Mittelkärnten und die Gurktaler Decke. *Mitt. Haus der Natur Salzburg* 17, 1–27.

Göd R.R. 1976: Petrologische Untersuchungen an einem alpinotypen Granitgneis und seinen Hüllgesteinen ("Villacher Granitgneis", Kärnten, Österreich*). Tschermaks Mineral. Petrograph. Mitt.* 23, 251–273.

Griem W., Wolf S., Sylvester H. & Thiedig F. 1991: Sedimentologie und Sedimentpetrographie des tertiären Sattnitzkonglomerats zwischen Villach und Klagenfurt (Kärnten, Österreich). *Jahrb. Geol. Bundesanst.* 134, 27–36.

Handler R., Velichkova S.H., Neubauer F. & Ivanov Z. 2004: $^{40}Ar/^{39}Ar$ age constraints on the timing of the formation of Cu–Au deposits in the Panagyurishte region, Bulgaria. *Schweiz. Mineral. Petrograph. Mitt.* 84, 1, 119–132.

Handler R., Ebner F., Neubauer F., Bojar A.V., Hermann S. 2006: $^{40}Ar/^{39}Ar$ dating of Miocene tuffs from the Styrian part of the Pannonian basin: first attempts to refine the Paratethys stratigraphy. *Geol. Carpath.* 57, 483–494.

Handy M.R., Ustaszewski., K. & Kissling., E. 2015: Reconstructing the Alps–Carpathians–Dinarides as a key to understanding switches in subduction polarity, slab gaps and surface motion. *Int. J. Earth Sci. (Geol. Rundsch.)* 104, 1–26.

Hanfland C., Läufer A.L., Nebelsick J.H. & Mossbrugger V. 2004: The Smrekovec Tertiary and related volcanism (Slovenia): sedimentology, geochemistry and tectonic evolution. *N. Jahrb. Geol. Paläont. Abhandl.* 232, 77–125.

Harangi S., Downes H.. Kósa L., Szabó Cs., Thirlwall M.F., Mason P.R.D. & Mattey D. 2001: Almandine garnet in calc-alkaline volcanic rocks of the Northern Pannonian Basin (Eastern-Central Europe): Geochemistry, petrogenesis and geodynamic implications. *J. Petrol.* 42, 1813–1844.

Harrison T.M., Célérier J., Aikman A.B., Hermann J., Heizler M.T. 2009: Diffusion of ^{40}Ar in muscovite. *Geochim. Cosmochim. Acta* 73, 1039–1051.

Heberer B., Reverman R.L., Fellin M.G.,Neubauer F., Dunkl I., Zattin M., Seward D., Genser J. & Brack P. 2017: Postcollisional cooling history of the Eastern and Southern Alps and its linkage to Adria indentation. *Int. J. Earth Sci.* 106, 1557–1580.

Hejl E. 1997: 'Cold spots' during the Cenozoic evolution of the Eastern Alps: thermochronological interpretation of apatite fission-track data. *Tectonophysics* 272, 159–172.

Hejl E. 1999: Über die känozoische Abkühlung und Denudation der Zentralapen östlich der Hohen Tauern — eine Apatit-Spaltspuranalyse. *Mitt. Österr. Geol. Ges.* 89 (1996), 179–199.

Heritsch H. 1964: Der Tonalitporphyrit von Reifnitz (Keutschach) südlich des Wörthersees. *Mitt. Naturwiss.. Ver. Steiermark 94*, 80–85.

Heritsch H. 1971: Neues zur Petrographie zweier Ganggesteine aus Kärnten*. Carinthia II Sonderheft* 28, 209–219.

Hoinkes G., Koller F., Rantitsch G., Dachs E., Höck V., Neubauer F. & Schuster R. 1999: Alpine metamorphism in the Eastern Alps. *Schweiz. Mineral. Petrogr. Mitt.* 79, 155–181.

Homann O. 1962: Die geologisch-petrographischen Verhältnisse im Raume Ossiachersee-Wörthersee (südlich Feldkirchen zwischen Klagenfurt und Villach). *Jahrb. Geol. Bundesanst.* 105, 243–272.

Hoskin P.W.O. & Schaltegger U. 2003: The composition of zircon and igneous and metamorphic petrogenesis. *Rev. Mineral. Geochem.* 53, 27–62.

Janák M., Froitzheim N., Yoshida K., Sasinkova V., Nosko M., Kobayashi T., Hirajima T. & Vrabec M. 2015: Diamond in metasedimentary crustal rocks from Pohorje, Eastern Alps: a window to deep continental subduction. *J. Metamorph. Geol.* 33, 495–512.

Kahler F. 1929: Karawankenstudien II. Die Herkunst des Sediments der Tertiärablagerungen am Karawanken-Nordrand. *Centr.-Blatt Min. Geol. Paläont., Abt. B* 1929, 6, 230–250.

Kahler F. 1931: Zwischen Wörthersee und Karawanken. *Mitt. Naturwiss. Ver. Steiermark* 68, 83–145.

Kahler F. 1953: Der Bau der Karawanken und des Klagenfurter Beckens. *Carinthia II, Sonderheft* 16, 1–77.

Kahler F. 1962: Geologische Karte der Umgebung von Klagenfurt 1:50,000. *Geologische Bundesanstalt*, Wien.

Kahler F. & Papp A. 1968: Über die bisher in Kärnten gefundenen Eozängerölle*. Carinthia II* 158, 78, 80–90.

Kázmér M. & Kovács S. 1985: Permian–Paleogene paleogeography along the Eastern part of the Insubric–Periadriatic Lineament system: Evidence for continental escape of the Bakony–Drauzug Unit. *Acta Geologica Hungarica* 28, 71–84.

Kirkland C.L., Smithies R.H., Taylor R.J.M., Evans N. & McDonald B. 2015: Zircon Th/U ratios in magmatic environs. *Lithos* 212–215, 397–414.

Kiss A. & Fodor L. 2007: The Csesznek Zone in the northern Bakony Mts: a newly recognised transpressional element in dextral faults of the Transdanubian Range, western Hungary. *Geol. Carpath.* 58, 465–475.

Kleinschmidt G., Heberer B. & Läufer A.L. 2008: Pre-Alpine sector-zoned garnets in the southeastern Alps. *Zeitschr. Deutsch. Ges. Geowiss.* 159, 565–573.

Kohút M. & Danišík M. 2017: Rapid cooling and geospeedometry of granitic rocks exhumation within a 1 volcanic arc: A case study from the Central Slovakian Neovolcanic Field 2 (Western Carpathians). *Island Arc* 26, DOI: 10.1111/iar.12201.

Koroknai B., Neubauer F., Genser J. & Topa D. 1999: Metamorphic and tectonic evolution of the Austroalpine units at the western margin of the Gurktal nappe complex, Eastern Alps. *Schweiz. Mineral. Petrogr. Mitt.* 79, 277–295.

Kralj P. 2012: Facies architecture of the Upper Oligocene submarine Smrekovec stratovolcano, Northern Slovenia. *J. Volcanol. Geotherm. Res.* 247–248, 122–138.

Kralj P. 2013: Submarine pyroclastic deposits in Tertiary basins, NE Slovenia. *Geologija* 56, 2, 187–197.

Kurz W., Wölfler A., Rabitsch R. & Genser J. 2011: Polyphase movement on the Lavanttal Fault Zone (Eastern Alps): reconciling the evidence from different geochronological indicators. *Swiss J. Geosci.* 104, 323–343.

Legrain N., Stüwe K. & Wölfler K. 2014: Incised relict landscapes in the eastern Alps. *Geomorphology* 221, 124–138.

Lippitsch R., Kissling E. & Ansorge J. 2003: Upper mantle structure beneath the Alpine orogen from high-resolution teleseismic tomography. *J. Geophys. Res.* 108, B8, 2376.

Lippolt J., Baranyi I. & Todt W. 1975: Das Kalium–Argon-Alter des Basaltes vom Lavant-Tal in Kärnten. *Der Aufschluß* 26, 238–242.

Liu X., Gao S., Diwu C. & Ling W. 2008: Precambrian crustal growth of Yangtse Craton as revealed by detrital zircon studies. *Amer. J. Sci.* 308*,* 421–468.

Ludwig K.R. 2003: ISOPLOT 3: a geochronological toolkit for Microsoft excel. *Berkeley Geochronology Centre Special Publication* 4, 1–74.

McDougall I. & Harrison T.M. 1999: Geochronology and thermochronology by the $^{40}Ar/^{39}Ar$ Method. *Oxford University Press*, Oxford, U.K., 1–269.

Meixner H. 1949: Laumontit aus dem Dioritporphyrit von Keutschach. *Karinthin* 5, 79–81.

Nemes F. 1997: Kinematics of the Periadriatic Fault in the Eastern Alps — Evidence from structural analysis, fission track dating and basin modelling. *Unpubl. PhD thesis, Faculty of Natural Sciences, University of Salzburg*, 1–225.

Nemes F., Neubauer F., Cloetingh S. & Genser J. 1997: The Klagenfurt Basin in the Eastern Alps: a decoupled intra-orogenic flexural basin? *Tectonophysics* 282, 189–204.

Neubauer F. 1987: The Gurktal Thrust System Within the Austroalpine Region: Some Structural and Geometrical Aspects. In: Faupl P. & Flügel H.W. (Eds.): Geodynamics of the Eastern Alps. *Deuticke*, Wien, 226–236.

Neubauer F. 2014: The structure of the Eastern Alps: from Eduard Suess to present-day knowledge. *Austrian J. Earth Sci.* 107, 1, 83–93.

Neubauer F. & Heberer B. 2011: Structural evolution of an extrusional wedge: constraints from a forgotten fault system in the Eastern Alps. In: GeoMunich 2011. FRAGILE EARTH: Geological Processes from Global to Local Scales and Associated Hazards (4–7 September 2011). *Abstracts with Programs, Geological Society of America*, A 24.

Neubauer F., Fritz H., Genser J., Kurz W., Nemes F., Wallbrecher E., Wang X. & Willingshofer E. 2000: Structural evolution within an extruding wedge: model and application to the Alpine–Pannonian system. In: Lehner F.K. & Urai J.L. (Eds.): Aspects of Tectonic Faulting (Festschrift in Honour of Georg Mandl). *Springer-Verlag,* Berlin–Heidelberg–New York, 141–153.

Oberli F., Meier M., Berger A., Rosenberg C. & Gieré R. 2004: U–Th–Pb and $^{230}Th/^{238}U$ disequilibrium isotope systematics: Precise accessory mineral chronology and melt evolution tracing in the Alpine Bergell Intrusion. *Geochim. Cosmochim. Acta* 68, 2543–2560.

Ogg J.G., Ogg G. & Gradstein F. M. 2008: The concise geologic time scale. *Cambridge University Press*, Cambridge, U.K., 1–177.

Pécskay Z., Lexa J., Szakács A., Seghedi I., Balogh K., Konečný V., Zelenka T., Kovacs M., Póka T., Fülöp A., Márton E., Panaiotu C. & Cvetković V. 2006: Geochronology of Neogene magmatism in the Carpathian arc and intra-Carpathian area. *Geol. Carpath.* 57, 511−530.

Pe-Piper G. 2000: Origin of S-type granites coeval with I-type granites in the Hellenic subduction system, Miocene of Naxos, Greece. *Eur. J. Mineral.* 12, 859–875.

Pfiffner O.A. 2014: Geology of the Alps. *Wiley-Blackwell*, Chichester, 1–392.

Piller W.E., Harzhauser M. & Mandic O. 2007: Miocene Central Paratethys stratigraphy — current status and future directions. *Stratigraphy* 4, 151–168.

Placer L. 2009: Tectonic subdivision of Slovenia. In: Pleničar M.M., Ogorelec B. & Novak M.: Geology of Slovenia. *Geološki Zavod Slovenije,* Ljubljana, 43–60.

Polinski R.K. & Eisbacher G.H. 1992: Deformation partitioning during polyphase oblique convergence in the Karawanken mountains, southeastern Alps. *J. Struct. Geol.* 14, 1203–1213.

Pomella H., Klötzli U., Scholger R., Stipp M. & Fügenschuh B. 2011: The Northern Giudicarie and the Meran-Mauls fault (Alps, Northern Italy) in the light of new paleomagnetic and geochronological data from boudinaged Eo-/Oligocene tonalites. *Int. J. Earth Sci. (Geol. Rundsch.)* 100, 1827–1850.

Pomella H., Stipp M. & Fügenschuh B. 2012: Thermochronological record of thrusting and strike-slip faulting along the Giudicarie fault system (Alps, Northern Italy). *Tectonophysics* 579, 118–130.

Ratschbacher L., Frisch W., Neubauer F., Schmid S.M. & Neugebauer J. 1989: Extension in compressional orogenic belts: The eastern Alps. *Geology* 17, 404–407.

Ratschbacher L., Frisch W., Linzer G. & Merle O. 1991: Lateral extrusion in the Eastern Alps, part 2: Structural analysis. *Tectonics* 10*,* 257–271.

René M. & Stelling J. 2007: Garnet-bearing granite from the Trebíč pluton, Bohemian Massif (Czech Republic). *Mineral. Petrol.* 91, 55–69.

Renne P.R., Balco G., Ludwig K.R., Mundil R. & Min K. 2011: Response to the comment by W.H. Schwarz et al. on "Joint determination of ^{40}K decay constants and $^{40}Ar^*/^{40}K$ for the Fish Canyon sanidine standard, and improved accuracy for $^{40}Ar/^{39}Ar$ geochronology" by P.R. Renne et al. (2010). *Geochim. Cosmochim. Acta* 75, 5097–5100.

Rieser A.B., Liu Y., Genser J., Neubauer F., Handler R., Friedl G. & Ge XH. 2006: $^{40}Ar/^{39}Ar$ ages of detrital white mica constrain the Cenozoic development of the intracontinental Qaidam Basin, China. *Geol. Soc. Amer. Bull.* 118, 1522–1534.

Romer R.L. & Siegesmund S. 2003: Why allanite may swindle about its true age. *Contrib. Mineral. Petrol.* 146, 297–307.

Rosenberg C.L. 2004: Shear zones and magma ascent: A model based on a review of the Tertiary magmatism in the Alps. *Tectonics* 23, TC3002.

Sachsenhofer R.F., Dunkl I., Hasenhüttl,Ch. & Jelen B. 1998: Miocene thermal history of the southwestern margin of the Styrian Basin: coalification and fission track data from the Pohorje/Kozjak area (Slovenia). *Tectonophysics* 297, 17–29.

Sandmann S., Herwartz D., Kirst F., Froitzheim N., Nagel T.J., Fonseca R.O.C., Münker C. & Janák M. 2016. Timing of eclogite-facies metamorphism of mafic and ultramafic rocks from the Pohorje Mountains (Eastern Alps, Slovenia) based on Lu–Hf garnet geochronometry. *Lithos* 262, 576–585.

Samadi R., Mirnejad H., Kawabata H., Harris C., Valizadeh M.V. & Gazel E. 2014: Magmatic garnet in the Triassic (215 Ma) Dehnow pluton of NE Iran and its petrogenetic significance. *Int. Geol. Rev.* 56, 596–621

Scaillet S. 2000: Numerical error analysis in $^{40}Ar/^{39}Ar$ dating. *Earth Planet. Sci. Lett.* 162, 269–298.

Schmid S.M., Zingg A. & Handy M.R. 1987: The kinematics of movements along the Insubric line and the emplacement of the Ivrea zone. *Tectonophysics* 135, 47–66.

Schmid S.M., Aebli H.R., Heller F. & Zingg A. 1989: The role of the Periadriatic line in the tectonic evolution of the Alps. In: Coward M.P., Dietrich D. & Park R.G. (Eds.): Alpine Tectonics. *Geol. Soc. Spec. Publ. London*, 45, 153–171.

Schoene B., Schaltegger U., Brack P., Latkoczy C., Stracke A. & Günther D. 2012: Rates of magma differentiation and emplacement in a ballooning pluton recorded by U–Pb TIMS-TEA, Adamello batholith, Italy. *Earth Planet. Sci. Lett.* 355–356, 162–173.

Schünemann M., von Gosen W. & Thiedig F. 1982: Die Viktringer Permotrias und ihre Beziehug zur Gurktaler Decke (Kärnten-Österreich). In: Thiedig F. (Ed.): Beiträge zur Stratigraphie, Metamorphose und Tektonik der Gurktaler Decke (Oberostalpin/Österreich). *Mitt. Geol.-Paläont. Inst. Univ. Hamburg* 53, 191–206.

Schwaighofer B. 1965: Zur Geologie und Petrographie des Altkristallins im südwestlichen Klagenfurter Recken (Kärnten). *Mitt. Geol. Bergbaustud. (Wien)* 16, 149–178.

Seghedi I. & Downes H. 2012: Geochemistry and tectonic development of Cenozoic magmatism in the Carpathian–Pannonian region. *Gondwana Res.* 20, 655–672.

Stipp M., Stünitz H., Heilbronner R. & Schmid S. 2002: The eastern Tonale fault zone: a 'natural laboratory' for crystal plastic deformation of quartz over a temperature range from 250 to 700 °C. *J. Struct. Geol.* 24, 1861–1884.

Thiedig F. 1970: Verbreitung, Ausbildung und stratigraphische Einstufung neogener Rotlehme und Grobschotter in Ostkärnten (Österreich). *Mitt. Geol.-Paläont. Inst. Univ. Hamburg* 39, 97–116.

Thiedig F. 1975: Die Entwicklung des postvariscischen Deckgebirges in der Umgebung der Saualpe. *Clausth. Geol. Abh., Sdbd.* 1, 175–186.

Thiedig F., van Husen D. & Pistotnik J. 1999: Geologische Karte der Republik Österreich 1:50,000, 186 Sankt Veit an der Glan. *Geologische Bundesanstalt*, Wien.

Trajanova M., Pécskay Z. & Itaya T. 2008: K–Ar geochronology and petrography of the Miocene Pohorje Mountains batholith (Slovenia). *Geol. Carpath.* 59, 247–260.

TRANSALP Working Group 2002: Gebrande H., Lüschen E., Bopp M., Bleibinhaus F., Lammerer B., Oncken O., Stiller M., Kummerow J., Kind R., Millahn K., Grassl H., Neubauer F., Bertelli L., Borrini D., Fantoni R., Pessina C., Sella M., Castellarin A., Nicolich R., Mazzotti A. & Bernabini M. 2002: First deep seismic reflection images of the Eastern Alps reveal giant crustal wedges and transcrustal ramps. *Geophys. Res. Lett.,* 29, 10, 92-1 – 92-4.

van Hinsbergen D.J.J., Straathof G.B., Kuiper K.F., Cunningham W.D. &Wijbrans J. 2008: No vertical axis rotations during Neogene transpressional orogeny in the NE Gobi Altai: coinciding Mongolian and Eurasian early Cretaceous apparent polar wander paths. *Geophys. J. Intern.* 173, 105–126.

Villa I.M. 2016: Diffusion in mineral geochronometers: Present and absent. *Chem. Geol.* 420, 1–10.

Villa I.M., Bucher S., Bousquet R., Kleinhanns I.C. & Schmid S.M. 2014: Dating polygenetic metamorphic assemblages along a transect through the Western Alps. *J. Petrol.* 55, 803–830.

von Blanckenburg F. & Davies J.H. 1995: Slab breakoff: A model for syncollisional magmatism and tectonics in the Alps. *Tectonics* 14, 120–131.

von Blanckenburg F., Kagami H., Deutsch A., Oberli F., Meier M., Wiedenbeck M., Barth S. & Fischer H. 1998: The origin of Alpine plutons along the Periadriatic Lineament. *Schweiz. Mineral. Petrogr. Mitt.* 78, 55–66.

von Gosen W. 1989: Gefügeentwicklungen, Metamorphosen und Bewegungen der ostalpinen Baueinheiten zwischen Nockgebiet und Karawanken (Österreich*). Geotekt. Forsch.* 72, 1–247.

von Gosen W., Pistotnik J. & Schramm J.-M. 1987: Schwache Metamorphose in Gesteinsserien des Nockgebietes und im Postvariszikum des Karawankenvorlandes (Ostalpen, Kärnten). *Jahrb. Geol. Bundesanst.* 130, 1, 31–36.

Wagner R., Rosenberg C.L., Handy M.R., Möbus C. & Albertz M. 2006: Fracture-driven intrusion and upwelling of a mid-crustal pluton fed from a transpressive shear zone — The Rieserferner Pluton (Eastern Alps). *Geol. Soc. Amer. Bull.* 118, 219–237.

Willingshofer W., Neubauer F. & Cloetingh S. 1999: Significance of Gosau basins for the upper Cretaceous geodynamic history of the Alpine–Carpathian belt. *Physics Chemistry Earth Part A: Solid Earth and Geodesy* 24, 687–695.

Wölfler A., Kurz W., Danišík M. & Rabitsch R. 2010: Dating of fault zone activity by apatite fission track and apatite (U–Th)/He thermochronometry: a case study from the Lavanttal fault system (Eastern Alps). *Terra Nova* 22, 274–282.

Wortel M.J.R. & Spakman W. 2000: Subduction and slab detachment in the Mediterranean–Carpathian region. *Science* 290, 1910–1017.

Yuan H.L., Gao S., Liu X.M., Li H.M., Günther D. &Wu F. Y. 2004: Accurate U–Pb age and trace element determinations of zircon by laser ablation-inductively coupled plasma mass spectrometry. *Geostandards Geoanalytical Res.* 28, 353–370.